

2-14-2014

PERMEABILITY AND MOISTURE DAMAGE CHARACTERISTICS OF ASPHALT PAVEMENTS

Mohiuddin Ahmad

Follow this and additional works at: https://digitalrepository.unm.edu/ce_etds

Recommended Citation

Ahmad, Mohiuddin. "PERMEABILITY AND MOISTURE DAMAGE CHARACTERISTICS OF ASPHALT PAVEMENTS."
(2014). https://digitalrepository.unm.edu/ce_etds/86

This Thesis is brought to you for free and open access by the Engineering ETDs at UNM Digital Repository. It has been accepted for inclusion in Civil Engineering ETDs by an authorized administrator of UNM Digital Repository. For more information, please contact disc@unm.edu.

Student Name: Mohiuddin Ahmad
Candidate

Graduate Unit (Department): Civil Engineering
Department

This thesis is approved, and it is acceptable in quality
and form for publication:

Approved by the Thesis Committee:

Rafiqul A. Tarefder, Chairperson

Percy Ng, Member

Mark Stone, Member

**PERMEABILITY AND MOISTURE DAMAGE CHARACTERISTICS OF
ASPHALT PAVEMENTS**

BY

MOHIUDDIN AHMAD

B.Sc. in Civil Engineering

Bangladesh University of Engineering & Technology, Dhaka, Bangladesh

THESIS

Submitted in Partial Fulfillment of the
Requirements for the Degree of

MASTER OF SCIENCE

Civil Engineering

The University of New Mexico
Albuquerque, New Mexico, USA

December 2013

© 2013, Mohiuddin Ahmad

DEDICATION

To my mom.

ACKNOWLEDGEMENTS

I would like to thank Dr. Rafiqul A. Tarefder for being my advisor and the thesis committee chair: for his support, time and advice throughout this study. I would also like to thank my thesis committee members: Dr. Percy Ng and Dr. Mark Stone for their advice and suggestions during this study.

This study is funded by New Mexico Department of Transportation (NMDOT). I would like to express my gratitude to Naomi Waterman and Shahidul Amin Faisal for their continuous support to finish the laboratory experiments. Special thanks go to NMDOT field exploration team for their help to conduct field testing and sample collection.

PERMEABILITY AND MOISTURE DAMAGE CHARACTERISTICS OF ASPHALT PAVEMENTS

by

Mohiuddin Ahmad

M.S. in Civil Engineering, University of New Mexico

Albuquerque, NM, USA 2013

B.Sc. in Civil Engineering, Bangladesh University of Engineering & Technology

Dhaka, Bangladesh 2007

ABSTRACT

In the past, numerous studies have been conducted on the topics of moisture damage and permeability, but very few studies have correlated permeability with moisture damage in Asphalt Concrete (AC). This study evaluates whether such a relation exists or not. In addition, correlations of permeability with AC mix volumetrics and pores are evaluated. Also, correlation of laboratory permeability with field permeability is examined.

In this study, a field survey is conducted to identify a set of eight pavements (bad) that are known to suffer from moisture damage and a set of eight pavements (good) that do not exhibit moisture damage. Field permeability testing is conducted on those 16 pavements. Results show that good performing pavements have very low (field) permeability compared to the bad performing pavements, which was expected. Field coring is conducted and cores are collected from all 16 pavement sections. Next, laboratory permeability testing is conducted on the field cores using a falling head permeameter. Based on laboratory permeability values, the good pavement sections exhibit smaller permeability than the bad performing sections.

To this end, moisture damage potential of field cores is determined in the laboratory using Moisture Induced Sensitivity Test (MIST) device and the AASHTO T 283 method. In MIST method, a sample is wet conditioned using repeated increase and decrease of pore pressure inside the saturated pores of AC sample. In the AASHTO T 283 method, a sample is wet conditioned using vacuum saturation and then subjected to one cycle of freeze-thaw. A set of three wet and three dry conditioned samples are tested for indirect tensile strength and Tensile Strength Ratio (TSR) of wet to dry sample sets is determined. It is shown that both MIST and the AASHTO T 283 yield TSR values of less than 1.0, which means moisture damage occurred by both conditioning methods. Based on the AASHTO T 283 data, when moisture damage is correlated with laboratory permeability, the AASHTO T 283 shows a good correlation but MIST shows a poor correlation. Correlations of field permeability with the AASHTO T 283 and MIST are found to be poor.

Mix volumetrics (e.g., gradation, porosity, binder content) tests are performed on field cores. Gradation data is plotted on a 0.45 power curve. Based on the power curve plot, it is shown that a mix gradation that passes near to the maximum density line have low permeabilities and moisture damage potentials.

It is known that an AC sample contains 3 types of pore: permeable, dead-end, and isolated pores. In this study, permeable pore is determined using a tracer test method, a concept borrowed from soil permeability testing. Dead-end and isolated pores are also determined using a CoreLok device. It is shown that permeable pores have a better correlation with permeability than the effective pore, which is defined as the sum of permeable and dead-end pores.

In this study, an attempt is made to correlate laboratory permeability with field permeability. Laboratory permeability does not have any correlation with the field permeability. This may be due to the fact that field permeability is affected by several factors such as 3D flow in the field, Open Graded Friction Coarse (OGFC), tack coats. To this end, an analytical model is developed to predict field permeability from laboratory permeability. Model permeability is found to be higher than the laboratory permeability. Because the model considers lateral and vertical direction flows whereas laboratory permeability test considers only vertical flow. It is shown that the model permeability is less than the field permeability for pavements with OGFC and more than the field permeability for pavements without OGFC. Therefore, a shift factor is developed to match the model permeability with the field permeability.

TABLE OF CONTENTS

Abstract	vi
List of Tables	xiii
List of Figures	xiv
Chapter 1	1
Introduction	1
1.1 Problem Statement	1
1.2 Objectives	5
1.3 Organization of the Thesis	5
Chapter 2	7
Literature Review	7
2.1 Introduction	7
2.2 Permeability Test Methods	7
2.2.1 Concept of Permeability Testing	7
2.2.2 Laboratory Methods	8
2.2.3 Field Methods	12
2.2.4 Arbitrary Methods	16
2.3 Factors Affecting Permeability	17
2.4 Predicting Field Permeability	17
Chapter 3	30

Experimental Design.....	30
3.1 Methodology.....	30
3.2 Survey.....	31
3.3 Field Testing Program.....	32
3.4 Test For Mix Volumetrics.....	33
3.5 Laboratory Permeability Testing.....	35
3.6 Moisture Damage Test.....	35
3.6.1 AASHTO T 283 Wet Conditioning.....	36
3.6.2 MIST Wet Conditioning.....	36
3.6.3 Tensile Strength Testing.....	37
Chapter 4.....	49
Correlating Permeability To Moisture Damage.....	49
4.1 Introduction.....	49
4.2 Test Matrix.....	49
4.3 Results and Discussions.....	50
4.3.1 Mix-volumetric.....	50
4.3.2 Field Damage with Field Permeability.....	51
4.3.3 Field Damage with Laboratory Permeability of Full Depth Samples.....	52
4.3.4 Field Damage with Laboratory Permeability of Samples Separated into Layers	52

4.3.5 MIST Damage with Permeability	53
4.3.6 AASHTO T 283 Damage with Permeability	54
4.3.7 Laboratory and Field Permeability	55
4.3.8 MIST and AASHTO T 283 Damage	55
4.3.9 Field Damage with Laboratory Damage	55
4.3.10 Laboratory Compacted Samples	56
4.4 Conclusions	57
Chapter 5	75
Field Permeability Model	75
5.1 Introduction	75
5.2 Tracer Test	75
5.3 Field Permeability Model	77
5.4 Selection of Candidate Pavement	82
5.5 Results and Discussion	82
5.5.1 Different Pores and Their Correlation with Permeability	82
5.5.2 Laboratory, Predicted and Field Measured Permeability	84
5.5.3 Quantification of Different Types of Pores and Their Relation with Moisture Damage	85
5.6 Conclusions	85
Chapter 6	95

Conclusions and Recommendations	95
6.1 Summary	95
6.2 Conclusions.....	98
6.3 Recommendations.....	99
References.....	100

LIST OF TABLES

Table 2.1	Different range of permeability and air voids	19
Table 2.2	NMAS and Related Permeability Values	20
Table 3.1	Participation of Districts from NMDOT	38
Table 3.2	Field permeability test locations	39
Table 3.3	Selected Pavements for Laboratory Testing	40
Table 4.1	Test Matrix	58
Table 4.2	Mix data for selected pavements	59
Table 4.3	Permeability Test Results	60
Table 4.4	TSR Calculation	62
Table 5.1	Pavement sections selected for tracer test	87

LIST OF FIGURES

Figure 2.1	Florida apparatus for permeability	21
Figure 2.2	Karol-Warner falling head permeability device	22
Figure 2.3	TxDOT permeameter	23
Figure 2.4	Pulse-decay permeability measurement	24
Figure 2.5	Kentucky air induced permeameter	25
Figure 2.6	NCAT field permeameter	26
Figure 2.7	ROMUS permeameter	27
Figure 2.8	Kuss Field Permeameter	29
Figure 3.1	Field permeability test set up	41
Figure 3.2	Field permeability test summary for US285 MP 140.53	42
Figure 3.3	Schematic of falling head permeameter	43
Figure 3.4	Different types of pores inside a HMA core sample	44
Figure 3.5	Bulk specific gravity of a cored sample	45
Figure 3.6	Laboratory permeability test	46
Figure 3.7	Sample in the MIST chamber	47
Figure 3.8	IDT testing in progress	48
Figure 4.1	Gradation curve for all pavement sections	64
Figure 4.2	Field permeability at different damage conditions	65
Figure 4.3	Laboratory full depth permeability at different damage conditions	66
Figure 4.4	Laboratory permeability of separated samples at different damage conditions	67

Figure 4.5	Correlation of MIST TSR permeability at different modes.	68
Figure 4.6	Correlation of AASHTO T 283 TSR permeability at different test modes	69
Figure 4.7	Permeability at different test modes	70
Figure 4.8	Comparison between AASHTO T 283 and MIST TSR	71
Figure 4.9	TSR values for good and bad performing pavement sections	72
Figure 4.10	Permeability vs. air voids	73
Figure 4.11	Permeability and moisture damage of labory compacted samples	74
Figure 5.1	Permeable pores and permeability set up	88
Figure 5.2	Breakthrough curve for a sample from NM344 at MP1.8	89
Figure 5.3	Different types of pores in a sample	90
Figure 5.4	Different types of pores and their correlation	91
Figure 5.5	Different permeabilities and their relation with pores	92
Figure 5.6	Comparison of field permeability with predicted and laboratory permeability	93
Figure 5.7	Different types of pores and their relation with moisture damage	94

CHAPTER 1

INTRODUCTION

1.1 PROBLEM STATEMENT

In the past, New Mexico Department of Transportation (NMDOT) has built asphalt pavements using dense-graded Hot Mix Asphalt (HMA) mixes. The initial in-place total pores (voids) of those dense graded mixtures are controlled not to be higher than eight percent and never fall below three percent during the life of the pavement. Higher pore content makes the pavement structure more permeable to air and water. High permeability may cause enhanced aging and moisture damage of HMA as well as endanger the subgrade and base courses. Lower pore content causes rutting and shoving due to shear deformation of mix constituents under repeated traffic loading. Thus, pores in an asphalt concrete pavement have contrasting effects on its properties and performance. Studies have shown that a dense graded mix containing total pores below 8% has low permeability (less than 100×10^{-5} cm/sec), which prevents infiltration of water inside a pavement (Mallick et al. 2001, Cooley and Brown 2000, Daniel et al. 2007). As a result, very little to no attention has been given so far to permeability of dense graded asphalt mixes nationally and in the state of New Mexico. This study determines permeability of sixteen pavement sections in New Mexico.

Moisture damage of asphalt pavement is an important issue worldwide. In the United States, the problem is also severe, as 34 out of 50 states are suffering from some sort of moisture related distress (Hicks 1991). According to Mogawer et al. (2002), 15 states reported moisture related problems out of 27 states surveyed. Moisture can enter inside

the pavement by three ways: infiltration, evaporation and capillary rise (Mercado 2007). In all cases, permeable pores provide the pathway for water to get inside the pavement. Moisture damage in asphalt can be prevented either by preventing water from entering an asphalt concrete (AC) or by strengthening the AC materials in the asphalt-aggregate system. Permeability is the way by which water can enter inside the pavement. This study evaluates whether the moisture damage in AC may be prevented or reduced by controlling permeability.

Very few studies have been conducted correlating permeability and moisture damage to this day. Choubane et al. (2007) has related degree of saturation with moisture damage. Moisture damage increases with the increase of saturation. Torres (2004) and Masad et al. (2006) divided air void content into three categories: low (impermeable), pessimum (intermediate) and free drainage. Maximum damage occurs at the intermediate range of permeability which corresponds to pessimum air void content. However, this has not been verified for different field conditions and test methods. Moisture damage of a pavement can be evaluated by two ways: visual inspection and mechanical testing. Stripping, which is one of the most common forms of moisture damage, generally occurs at interfaces and propagates upward. Therefore, it is difficult to identify moisture damage by visual inspection only (Kim and Coree 2005). Mechanical methods used are the AASHTO T 283 (AASHTO 2007), Moisture Induced Sensitivity Testing (MIST), Nottingham asphalt test equipment, Hamburg wheel test, etc. Among them, the AASHTO T 283 is the most widely used and experimented method. In the AASHTO T 283 method, samples are vacuum saturated and subjected to freeze-thaw. However, it is time consuming and the variable degree of saturation may affect the test result. The pore

pressure cycles, as in the field due to wheel passing on moist pavement, are not simulated in this method (Liang 2008). The recently developed MIST device can simulate pore pressure cycles (MIST 2012). In this study, both the AASHTO T 283 and MIST are used to cause moisture damage to AC samples in the laboratory.

Past studies show that permeability increases exponentially with the increase in total pores in HMA samples (Retzer 2008, Mallick et al. 2003, Vivar and Haddock 2007, Cooley et al. 2002, Hainain et al. 2003, Ahmad and Tarefder 2013). Total pore consists of three pores: permeable pore, dead-end pore, and isolated pore (Tarefder and Zaman 2005). Only pores that continue from the top to the bottom of a sample are responsible for permeability (i.e., conduction of flow) and therefore they are called permeable pores. Permeable pores and dead-end pores are accessible by water and therefore, sum of these two pores are also known as effective pores (Bear 1972). Effective pore in an AC sample is always less than the total pores (Koponen et al 1997). Effective pores can be determined using a Corelok™ device as per ASTM D 6752. In fact, Corelok™ device measures both bulk and apparent specific gravities. The percent difference in specific gravities normalized by the apparent specific gravity gives the effective pores (Vivar and Haddock 2005, Bhattacharjee and Mallick 2002). In the past, most studies concluded that a poor correlation exists between the total pore and permeability. Permeability specifications of some state Department of Transportation (DOTs) are also based on the total pores and permeability correlation. Some studies have shown that effective pores show a better correlation with permeability (Bear 1973, Bhattacharjee and Mallick 2002), as isolated pores are eliminated from total pores. However, effective pores include dead-

end pores, which have little or no contribution to permeability (Bear 1973). Ideally, one should correlate permeable pores to permeability.

As flow occurs only through permeable pores, it is necessary to measure it, which is done in this study. Ranieri et al. (2010) determined pores using X-ray tomography and correlated it to permeability. Liang et al. (2000) used image processing to determine pores in rocks. Omari (2004) used X-ray CT images to evaluate pores of HMA cores. While these methods are very advanced and sometimes complex, a tracer method, which has been successfully used for soils permeability (Rogowski 1988, Yeh et al. 2000, Stephens et al 1998), can be useful and therefore tried in this study to determine permeable pores in AC.

Although permeability of HMA pavement is measured both in the field and laboratory, correlating laboratory permeability with field permeability is very difficult. In the laboratory, permeability test sample confined at the sides and flow is regulated one-dimensionally, which is different from the field permeability boundary condition. Some researchers tried to correlate laboratory permeability to field permeability (Keniptong et al 2005), but those studies did not succeed and were based on experiments only. Field permeability is affected by several variables such as degree of saturation, boundary conditions, flow directions, etc. (Gogula et al 2004). Thus field measured permeability value is always found to be either less or more than the laboratory permeability of AC sample. For example, during field permeability testing in this study, it was clearly observed that if a field HMA layer is covered by an Open Graded Friction Course (OGFC), water mostly flow laterally through the OGFC layer during field permeability testing. Water flow through the OGFC yields a very high permeability, which is not the

representative permeability of the HMA layer. In other cases, if field HMA layers contain a seal coat, tack coat, and prime coat, these coats retard the vertical flow during field permeability testing and yield a very low permeability, which is also not the true permeability of the HMA layer. Therefore, field permeability test results need to be evaluated cautiously. Saturation is another issue but needed for a successful permeability testing in the field. One can use air permeameter, which can eliminate the problem associated with degree of saturation to some degree (Menard and Croveti 2006). However, it still has other limitations such as different coatings and boundary conditions. In addition, sometimes it is difficult to set up field permeability tests due to bad weather, a lack of field crews, and required traffic control. This study attempts to develop an analytical model to predict field permeability from laboratory core permeability test results.

1.2 OBJECTIVES

The main objectives of this study are to:

- Find whether permeability is related to moisture damage of AC.
- Measure permeable pores in AC and its relation to permeability.
- Relate field permeability with laboratory permeability.

1.3 ORGANIZATION OF THE THESIS

This thesis consists of six chapters. Chapter 1 defines the problem of permeability and moisture damage in AC. Chapter 2 contains literature review on different laboratory and field permeability test methods, factors affecting permeability, permeability practices of different states and countries. Chapter 3 contains experimental plan for this study, field

and laboratory testing performed during this study. Chapter 4 describes the correlation between permeability and moisture damage. Chapter 5 determines the permeable pores and an analytical model to determine field permeability from testing cores in the laboratory. Chapter 6 summarizes the findings of this study.

CHAPTER 2

LITERATURE REVIEW

2.1 INTRODUCTION

The author conducted a comprehensive search of databases and various information sources (like journals, research reports, standards) to build a solid base of knowledge on current research. Particular emphasis was placed on permeability testing methods. Review of the factors affecting permeability is also made.

2.2 PERMEABILITY TEST METHODS

2.2.1 Concept of Permeability Testing

Permeability or hydraulic conductivity of a material refers to its ability to transmit water through it. It is obtained from Darcy's law: flow velocity is proportional to hydraulic gradient.

$$V \propto i$$

$$V = ki \tag{2.1}$$

where V = flow velocity (cm/s); i = flow gradient defined by head loss over sample length; k = permeability of the sample (cm/s).

Therefore, discharge rate (Q) will be:

$$Q = AV = kiA \tag{2.2}$$

where Q = discharge (cm³/s) and A = cross section area (cm²).

Permeability of soil is determined either using falling head or constant head permeameter. Almost all permeameter are based on one of these two mechanisms.

Permeability of asphalt is evaluated both in the field and in the laboratory. Different states or organizations used different instruments to determine permeability. Brief descriptions of them are given in next sections.

2.2.2 Laboratory Methods

Florida Method of Permeability

Scope: This test method covers the laboratory determination of the water conductivity of compacted asphalt paving mixture sample. The measurement provides an indication of water permeability of that sample as compared to those of other asphalt samples tested in the same manner. The procedure uses either laboratory compacted cylindrical specimens or field core samples obtained from existing pavements.

Summary of the Test Method: A falling head permeability test apparatus is used to determine the rate of flow of water through the specimen. Water in a graduated cylinder is allowed to flow through a saturated asphalt sample and the interval of time taken to reach a known change in head is recorded. The coefficient of permeability of the asphalt sample is then determined based on Darcy's Law.

Significance and Use: This test method provides a means for determining water conductivity of water-saturated asphalt samples. It applies to one-dimensional, laminar flow of water. It is assumed that Darcy's law is valid.

Calculations: The coefficient of permeability, k , is determined using the following equation:

$$k = \frac{aL}{At} \ln \left(\frac{h_1}{h_2} \right) \times t_c \quad (2.3)$$

where k = coefficient of permeability, cm/s; a = inside cross-sectional area of the burette, cm²; L = average thickness of the test specimen, cm; A = average cross-sectional area of the test specimen, cm²; t = elapsed time between h_1 and h_2 , s; h_1 = initial head across the test specimen, cm; h_2 = final head across the test specimen, cm; t_c = temperature correction for viscosity of water.

Oklahoma Method of Permeability

Scope: This test method covers the laboratory determination of permeability of the compacted asphalt paving mixture sample. The sample is either lab compacted or collected field cores.

Summary of the Test Method: Evacuate air from the sealing tube. Place the specimen on top of the lower plate. Place the sealing tube over the specimen. Insert the upper cap assembly it into the sealing tube. Install the clamp assemble onto the permeameter frame. Inflate the membrane and pour water in the graduated cylinder and shake to remove air. Fill again up to initial timing mark. Start the timing device and record total time taken by water to reach the lower meniscus.

The coefficient of permeability, k , is determined using Eq. (2.3).

Karol-Warner Falling Head Permeability Device

Description: In this falling head permeability test, as outlined in the ASTM provisional standard PS-129, a saturated asphalt sample is sealed on the sides and placed under a column of water so that water can only flow through the sample. The time required for the water column to experience a specified change in elevation is determined. The test is

repeated until four consecutive readings do not differ by more than ten percent. This process confirms that the sample was, in fact, saturated. Otherwise, it would be unclear whether movement of the water column was due to water infiltrating void spaces or actual flow through the sample (Williams, et al. 2006).

Calculation: The permeability for water is calculated using the following equation,

$$k = \frac{aL}{At} \ln \left(\frac{h_1}{h_2} \right) \quad (2.4)$$

TxDOT Permeability Method

Scope: This test procedure to measures the time of water flow through laboratory compacted specimens. Then permeability is determined.

Apparatus: Cylindrical laboratory permeameter, stop watch.

Specimen: 6 in. diameter 4.5 in. height lab compacted sample or field core of 6 in. diameter and height not more than 4.5 in.

Procedure: The test specimen is placed inside the cylindrical laboratory permeameter. Rubber clamps around the permeameter are secured at the top and bottom edges of the test specimen. The clamps are placed such that the top and bottom edges are approximately in the middle of the location of the clamps. The permeameter is filled with water approximately 1–2 in. above the top marking on the pipette. The timing device is started when the water level reaches the top marking on the pipette. The timing is stopped when the water level reaches the bottom marking on the pipette. The time taken by water to travel from the top marking to the bottom marking is recorded. Permeability is calculated by falling head formula.

Pulse-Decay Method of Permeability

Introduction: The system consists of an upstream reservoir of volume V_1 , a sample holder and a downstream reservoir of volume V_2 . A differential pressure transducer measures the pressure difference between the reservoirs and another transducer measures the pressure p_2 in the downstream reservoir. No flow measurement device is required. Flow rate can be calculated from known volume of each reservoir, fluid compressibility and rate of pressure change.

Procedure: High pressure is applied at upstream reservoir with all bulbs open. When pressure become uniform all over the system, upstream pressure is increased keeping bulbs such way that pressure pulse enters into the sample. The upstream pressure will decrease with time and downstream pressure will increase until the pressure difference become zero. The pressure difference is measured with time and plotted in a semi-log plot. The slope of the line could be obtained by:

$$|Slope| = \frac{6.805 \times 10^{-5} f_1 A k_L}{\mu_L (c_L + c_{V_1})} \left(\frac{1}{V_1} + \frac{1}{V_2} \right) \quad (2.5)$$

$$\text{Hence, } k_L = \frac{-14696 m \mu_L (c_L + c_{V_1})}{f_1 A \left(\frac{1}{V_1} + \frac{1}{V_2} \right)} \quad (2.6)$$

where m = slope; μ_L = viscosity of the liquid, cp; c_L = liquid compressibility, psi^{-1} ; c_{V_1} = compressibility of upstream reservoir, psi^{-1} ; f_1 = mass-flow correction factor; A = cross section area of the cylindrical sample, cm^2 .

This method is used normally for rock permeability measurement.

Faster Pulse Decay Permeability Measurement

Description: The method is similar to that described in previous method, except the pressure equilibrium step is eliminated and the test can be performed quicker than before. And two additional reservoirs are added to the previous instrument.

2.2.3 Field Methods

California Method of Permeability

Scope: This method describes the procedure for determining the permeability of bituminous pavements and seal coats.

Test Procedure: A 6 in. diameter circle on pavement surface is drawn, small amount of grease is pushed on pavement, and cylinders are filled with test solution. The valve at the base of the special plastic graduated cylinder is released. The special plastic cylinder is refilled from the polyethylene graduate if more solution is needed during the test. At the end of the 2-minute test period, the total amount of solution used is determined.

Calculation: The total quantity of solution used during the test period is divided by two and the result is shown as the relative permeability in mL/min.

Kentucky Method

Scope: This method describe the procedure for determining in place permeability of an HMA mat using an air induced permeameter. This method is applicable for all nominal maximum size and gradation.

Apparatus: Permeameter, Air compressor and caulking gun.

Procedure: The air compressor is connected to the multi venture vacuum cube. Approximately a one-half inch bead of silicon rubber caulk is applied; one inch inside the outer edge of sealing ring. The permeameter is placed in the center of the area to be

tested. No more than 50 pounds of load is applied on permeameter and twist. The bulb of multi-venturi vacuum cube is opened to permit the flow of air. The reading on the digital vacuum will begin to increase. When this number reaches to peak, the test is finished and the bulb can be shut. Test time should not exceed 15s. The highest reading attained by the permeameter is recorded by pressing the button marked “HI/LO”.

Calculation: Permeability of the mat in ft/day may be calculated from the following equation,

$$k = 255757.53V^{1.556} \quad (2.7)$$

where k = permeability in ft/day; V = vacuum reading in mm Hg

TxDOT Procedure for Field Permeability

Scope: This empirical test procedure is used for pavements under construction or on roadways already constructed to test and verify that the compacted mixture has adequate permeability.

Apparatus: Cylindrical field permeameter, stop watch and Plumber’s putty.

Procedure: The permeameter is placed on the pavement surface using putty to seal it with pavement. The permeameter is filled 1-2 inch more than top marking. Time taken by water to travel from top marking to bottom marking is recorded. Time is normally less than 20s for newly constructed pavement. Permeability is calculated using falling head method.

NCAT Field Permeameter

Scope: This test method covers the in-place estimation of the water permeability of compacted hot mix asphalt (HMA) pavement.

A falling head permeability test is used to estimate the rate at which water flows into a compacted HMA pavement. Water from a graduated standpipe is allowed to flow into a compacted HMA pavement and the interval of time taken to reach a known change in head loss is recorded. The coefficient of permeability of a compacted HMA pavement is then estimated based on Darcy's Law.

Significance and use: This test method provides a means of estimating water permeability of compacted HMA pavements. The estimation of water permeability is based upon assumptions that the sample thickness is equal to the immediately underlying HMA pavement course thickness; the area of the tested sample is equal to the area of the permeameter from which water is allowed to penetrate the HMA pavement; one-dimensional flow; and laminar flow of the water. It is assumed that Darcy's law is valid (Cooley et al. 1999).

Calculation: Same formula used for any falling head method.

ROMUS Air Permeameter

Description: The ROMUS air permeameter uses air that is gathered from the atmosphere as the fluid to measure permeability. The machine has a vacuum pump that operates on a rechargeable battery and depressurizes the tank to negative 24 inches of head. When the test is ready to begin, the air tank is pressurized to 24 inches of head if it is not already at the appropriate pressure. The air is then drawn through the pavement surface while a pressure sensor checks the pressure in the tank. At every 4 inches of pressure drop the time is recorded. The time is the only output for the device (Retzer et al. 2008).

Calculation: Permeability of the pavement is calculated from the following equation which is modified from falling head equation:

$$k_w = \left[\frac{LV\mu\rho_w g}{TAP_a\mu_w} \right] \ln \left(\frac{p_1}{p_2} \right) \quad (2.8)$$

where k_w = hydraulic permeability ,cm/s; L = pavement layer thickness cm; V = volume of vacuum chamber (cm^3); μ = kinematic viscosity of air (gm/cm/s); ρ_w = density of water (gm/cm^3); g = gravitational acceleration (cm/s^2); T = time of head drop (s); A = area of being tested (cm^2); P_a = pressure (atmospheric) (Ba); μ_w = kinematic viscosity of water (gm/cm/s); p_1 = initial pressure (Ba); p_2 = final pressure (Ba).

The Kuss Field Permeameter

Description: The Kuss Field Permeameter (KSFP) operates using the constant head approach. To do this, a patented gas-measurement system is used to measure the amount of air needed to replace the water in order to maintain a constant pressure head. When the test begins, water is allowed to flow from the standpipe and cover the pavement testing surface to a depth of approximately 1 in. A sensor is used to monitor the water level, and is connected to a flow valve in the flow meter box. As water infiltrates the pavement, the water level over the pavement drops, and the sensor alerts the flow valve, allowing air to enter the standpipe above the water column. This metered volume of air acts as a substitute for the head pressure originally applied by the water, thereby maintaining a constant head. A data acquisition system measures and records the flow rate of water through the pavement over time, and the permeability is calculated using the rate of flow of water into the pavement and the cross-sectional area of the pavement test section. The relationship is presented in Equation below, (Williams et al. 2006):

$$k = \frac{Q}{60 \left(\frac{2.54 + L}{L} \right) A} \quad (2.9)$$

where k = coefficient of permeability, cm/s; Q = flow rate, cm³/min; A = area of base plate, 1264.5cm²; L = pavement thickness, cm.

Double Ring Infiltrometer

The double ring infiltrometer test is performed as per ASTM D 3385 and mainly used for soils. Two 20 in. high ring of 12 in. and 24 in. diameter are used. The rings are driven to the soft ground around 6 in. Water flow by the outer ring forces the water flow through inner ring in perpendicular direction only. The infiltration rate of the inner tube is measure. However, it is difficult to use the infiltrometer for asphalt pavements as it can't be driven inside the pavement.

2.2.4 Arbitrary Methods

Modified Kozeny-Carman equation

$$k = \frac{V_a^m}{c.S_{agg}^t} \frac{\gamma}{\mu} \quad (2.10)$$

where V_a^m = % air void; γ = 9.79 kN/m³; μ = fluid viscosity. (Masad et al. 2002)

The permeability coefficient of an asphalt mixture can be estimated by the following equation (Arkansas Highway Transportation Department (1998)):

$$k = 1.38 \times 10^{-7} \times 3.92^{\%V_a} \times 0.61^t \quad (2.11)$$

where $\%V_a$ = Air Voids, expressed as a percentage; t = lift thickness (Willoughby, et all. 2001).

2.3 FACTORS AFFECTING PERMEABILITY

Research conducted by the NCHRP showed an inverse relationship between VMA and mixture permeability, i.e. for a given air void content permeability decreased as the VMA increased (Brown et al. 2004). Also, with increase in coarse aggregate, permeability also increased. One reason for such increase is increase of interconnected air voids. Superpave mixes tend to have this trait as well as having a larger NMA with lesser fines to fill void spaces which results in a substantial increase in permeability (Vivar 2007). Void contents as low as 4.4% have been shown adequate for 25 mm NMA mixes and 7.7% being the maximum for NMA mixes of 9.5 mm. Table 1 shows air permeability ranges at different air voids.

Permeability increases with an increase of NMA. Mallick et al. 2003 got permeabilities for 6 percent air void as shown in Table 2.

Another factor that influences permeability is gradation. For coarse graded mix, because of coarser particles, the void size is larger resulting more interconnected void. According to Mallick et al, lift thickness (or t/NMA) also affects permeability. As thickness (or t/NMA) increases, the potential for interconnected air void decreases, resulting decreases in permeability.

2.4 PREDICTING FIELD PERMEABILITY

Kanitpong et al. (2005) performed many field tests for permeability and lab test of lab compacted sample of same mix design to relate field and lab permeability value. He also correlated field permeability by field test method with field permeability by lab test. He gave the following correlation of field permeability and lab permeability of field cores:

$$P8 > 45\%, \quad \text{Field } K = 8.34 \times e^{0.055(\text{Lab } k)} \quad R^2 = 0.80 \quad (2.12)$$

$$40 < P8 < 45\%, \quad \text{Field } K = 21.68 \times e^{0.039(\text{Lab } k)} \quad R^2 = 0.49 \quad (2.13)$$

where $P8$ is the percent passing through No.8 sieve. No correlation was found for other mixtures.

To determine correlation between field permeability with lab compacted sample permeability, he described two methods.

Method A: First, G_{mb} of field core is determined. Then amount of material needed to produce lab sample of same height and density were determined using the following equation,

$$W_t = G_{mb} \times t \times \frac{A}{1000} \quad (2.14)$$

where W_t = amount of material, gm; t = height or thickness of the field cores, mm; A = cross section area of the specimen, mm^2 .

The SGC sample was compacted using the Superpave Gyratory Compactor, fixing the height. The permeability of these samples were predicted and found less than that obtained from field cores. And the relation is described by:

$$y = 22.24 + 0.73x \quad R^2 = 0.6 \quad (2.15)$$

where y = lab permeability of field cores (cm/s); x = lab permeability of SGC sample (cm/s).

Method B: Here mixes are collected from field and N_{des} was fixed for all samples. So, densities of the samples were different. Then, permeability of the samples was

determined using ASTM D5084. And permeability vs. density curve was plotted for SGC samples of method B. From this plot, permeability corresponding to field density was determined. Finally, predicted permeability and measured permeability of field cores were plotted on a graph which gives almost a straight line of slope 1. That indicates the Permeability determined by method B was equal to the permeability of field cores.

Table 2.1 Different range of permeability and air voids

k (cm/s)	Description of Permeability	Description of Air Voids
$<10^{-4}$	Impervious-Impermeable	$<5\%$
$10^{-4}-10^{-2}$	Poor drainage-Permeable	5-7%
10 ⁻² or higher	Good Drainage-Very Permeable	$>7\%$

Table 2.2 NMAS and related permeability values

NMAS(mm)	Permeability(cm/s)
9.5	6×10^{-5}
12.5	40×10^{-5}
19.0	140×10^{-5}
25.0	1200×10^{-5}



Figure 2.1 Florida apparatus for permeability



Figure 2.2 Karol-Warner falling head permeability device

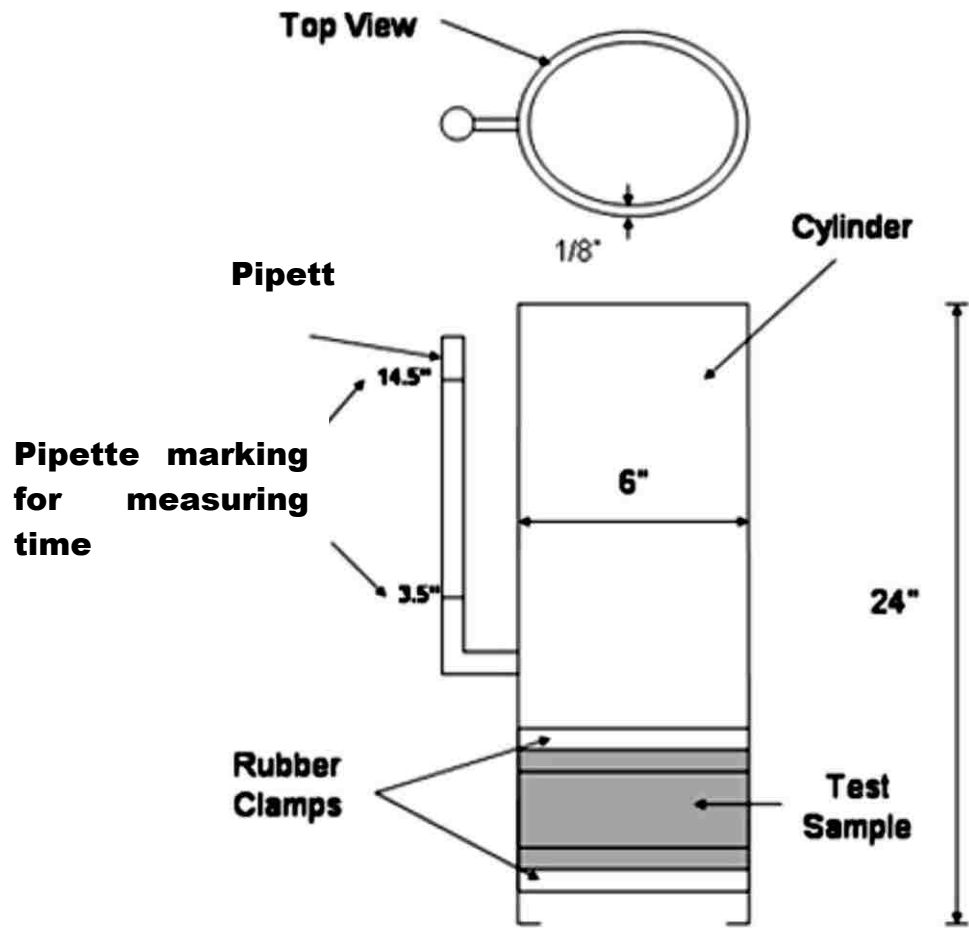
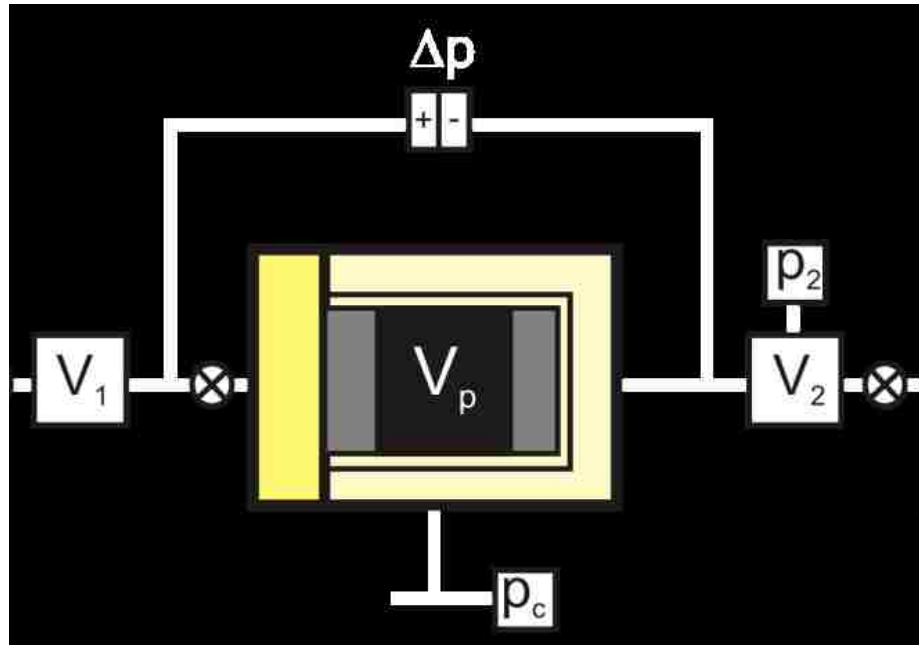
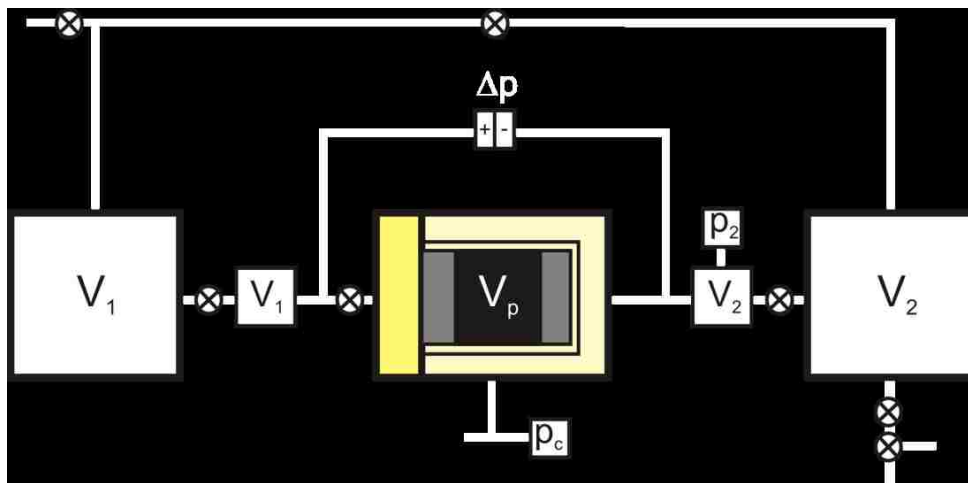


Figure 2.3 TxDOT permeameter



(a) Pulse-decay measuring apparatus



(b) Faster pulse-decay measuring apparatus

Figure 2.4 Pulse-decay permeability measurement



Figure 2.5 Kentucky air induced permeameter

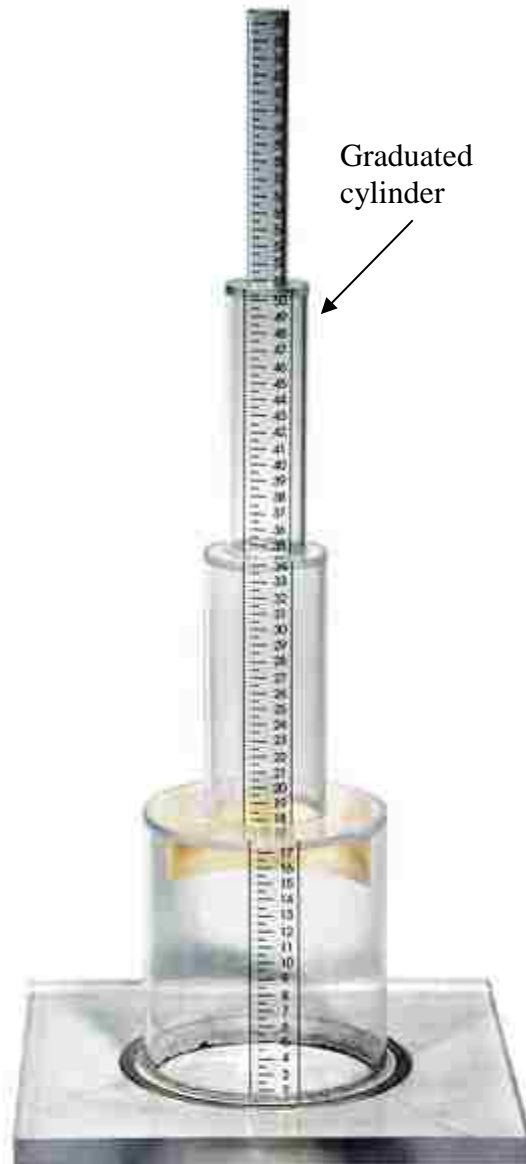


Figure 2.6 NCAT field permeameter

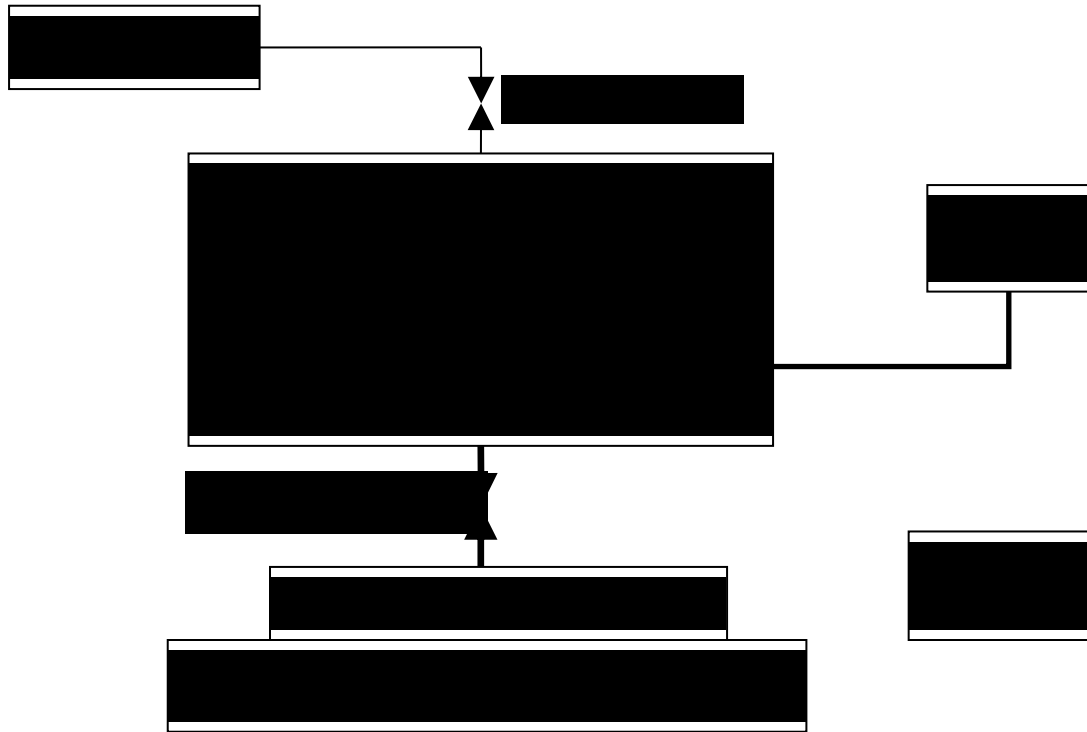


Figure 2.7 ROMUS permeameter

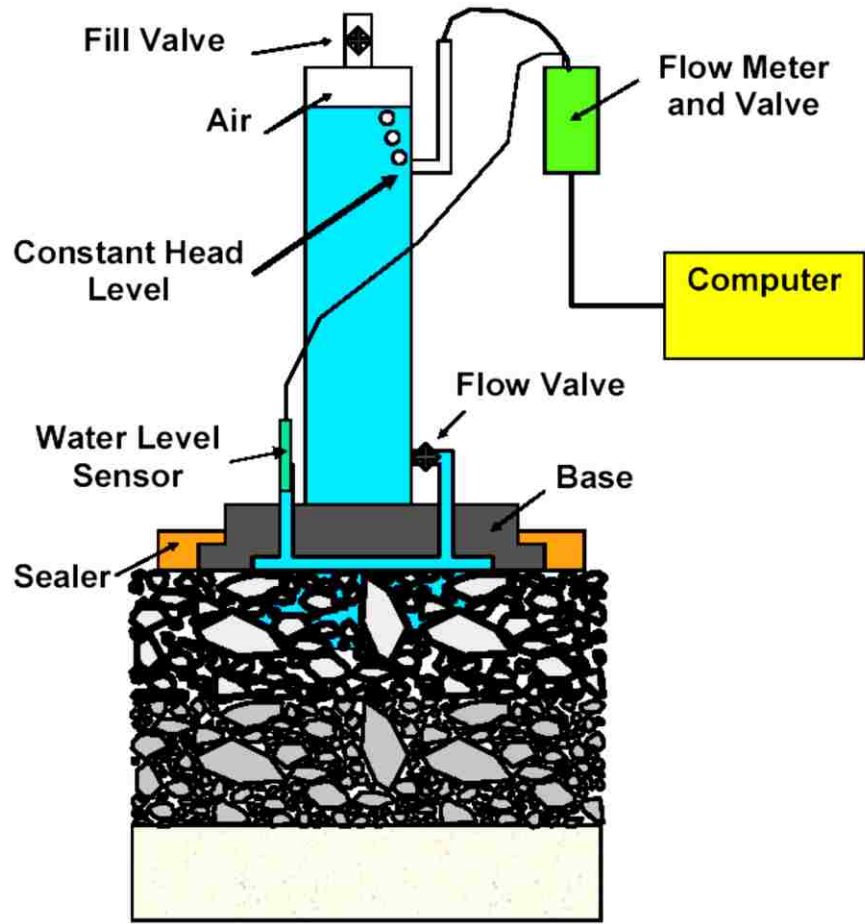


Figure 2.8 Kuss field permeameter

CHAPTER 3

EXPERIMENTAL DESIGN

3.1 METHODOLOGY

The experimental plan for this study is shown in Figure 3.1. A field survey was conducted in cooperation with New Mexico Department of Transportation (NMDOT). The main objective of the field survey was to identify a set of bad (moisture damaged) and good (undamaged) performing asphalt pavement sections.

Field permeability tests were performed on those sections using an NCAT field asphalt permeameter. In New Mexico, most of the pavements are surfaced with open graded friction course (OGFC). Therefore, permeability testing and field coring were conducted on the shoulder, which is not typically treated with OGFC.

Florida apparatus using the falling head permeability test method determined laboratory permeability values of full depth cores. Ideally, full depth laboratory permeability should be compared to field permeability. The cores were separated by layers using a laboratory wet saw. Permeability tests were performed on the samples representing individual layers.

Moisture damage on samples separated by layers was evaluated by a ratio of the indirect tensile strength of a set of wet samples to that of a set of dry samples. In this study, wet conditioning was performed by two methods: the AASHTO T 283 (AASHTO 2007) and a recently developed MIST device. The difference between the AASHTO T 283 and MIST conditioning is that the AASHTO T 283 causes damage to the AC sample by

freeze-thaw action and MIST causes damage to the AC sample by increasing and releasing pore pressure inside the sample. In both cases, temperature is 60 °C.

3.2 SURVEY

The survey questioner was set by the distributed to 42 NMDOT employees from all six of the NMDOT districts. The survey was followed by phone calls to spur the response.

Below are the two questionnaires' of the survey.

- Is there a section (or project) of a roadway/pavement that shows moisture wicking in your district? Basically, if you know about a pavement section that does not get dried up in few hours (say couple of hours) after a short rainfall. If such, what is causing the above problem (high permeability, stripping, roadway drainage problem, moisture damage, etc.)?
- Can you mention couple of pavement sections that are performing very well in terms of permeability or drainage or moisture damage or stripping issue? Milepost or location will be helpful.

Survey Response Synthesis and Data Collection

Except district 1 and 4, all other four districts answered the survey questions. Based on their answers, pavements with high permeability or showing visual stripping are classified as bad performing pavement. On the other hand, pavements with low permeability or no visual stripping are grouped as bad performing pavements. List of good and bad performing sections are shown in Table 3.1.

3.3 FIELD TESTING PROGRAM

Based on the survey, field permeability tests were performed on the locations shown in Table 3.2.

Procedure for the field testing followed by the UNM research team includes a field inspection of drainage, measurement and sketch of the lane markings and characteristics of the section including width of lanes, shoulder, wheel path location and distance from the shoulder stripe. The drainage is determined by the measurement of the slope and inspection of the crown design. The team then lays down a template around the tape marks from the FWD testing that the NMDOT team has performed at the section location. The holes are marked with construction crayon and the team determines which will be used for field testing and proceeds to testing. After the tests are performed, the NMDOT team cores the 24 holes that were marked by the UNM research team. 12 6" diameter cores and 12 4" diameter cores were taken and cataloged by the NMDOT team. Figure 3.1 shows the field permeability test set up. Figure 3.2 show schematics of a section from District 2 that were tested March 14-15, 2012. Figure 3.3 describes the falling head permeability mechanisms.

NCAT field asphalt permeameter is used to determine field permeability value using Eq. (2.4).

In the field, a crack-free spot is selected to place the permeameter. This area is then cleaned using a broom. Next, a wax ring is placed at the base of the permeameter, which is then placed on the cleaned area. The base is pushed downward so that the wax ring is attached to the pavement without any water leaking. Three 10 lb. weights are then placed on the permeameter base to resist it from uplift pressure by water. Water is poured inside

the tube and it is allowed to flow for a few minutes to saturate the pavement. Figure 3.1 shows a field permeability test set-up. Though Eq. (2.4) is used for field permeability value, flow occurs both in vertical and lateral directions in the field. An impermeable or incompatible middle layer can direct the flow along the lateral direction. The permeability test was conducted around noon time. It is possible that a thermal gradient exists along the thickness of the Hot Mix Asphalt (HMA) pavements, which may affect the flow. However no temperature correction is considered for field permeability calculations.

Core Collection and Selection of Candidate Pavements for Laboratory Testing

A total of 24 cores were collected from each of the 23 locations. The cores were inspected to see if there exists any stripping at the interface of the layers. Depending on the visual inspection the pavements were classified as good or bad performing as shown in Table 3.3. The number assigned to each pavement and number of layer each pavement has are also shown in this table.

3.4 TEST FOR MIX VOLUMETRICS

The total air void a sample has is termed as total pores. It consists of permeable pores, isolated pores, and dead end pores. Permeable pores and dead end pores are accessible by water and termed as effective pores. These pores are shown in Figure 3.4.

Bulk specific gravity of a cored sample is determined using Corelok™ device as per ASTM D 6752. Dry weight of the sample is measured. Sample is placed inside a plastic bag of known weight and specific gravity and placed inside the Corelok™ device. Air from the Corelok chamber is sucked out and the polybag is sealed as shown in Figure 3.5.

The underwater weight of the sample with polybag is measured. The bag is cut open under water and the weight is recorded again. Bulk specific gravity of the sample is calculated from Eq. (3.1):

$$G_{mb} = \frac{A}{A + D - B - D/F} \quad (3.1)$$

where A = sample dry weight in air, gm; D = polybag weight in air, gm; B = weight of sealed sample in water, gm; F = specific gravity of polybag at 25 °C.

Apparent specific gravity is determined using Eq. (3.2):

$$G_{ma} = \frac{A}{A + D - C - D/F} \quad (3.2)$$

where C = weight of sealed sample and polybag cut under water.

Effective pores are determined using Eq. (3.3) as follows:

$$n_e = \frac{G_{ma} - G_{mb}}{G_{ma}} \quad (3.3)$$

After all tests are done on a sample, it is placed inside the oven to prepare loose mix. Maximum specific gravity is determined using Corelok device as per ASTM D6857. Weight of loose mix and polybag is measured. The loose mix is placed inside the polybag and vacuum sealed. The bag is cut opened under water and water saturates the mix. The weight is measured. Maximum specific gravity is then determined by Eq. (3.4):

$$G_{mm} = \frac{A}{A + D - C - D/F} \quad (3.4)$$

A = loose mix dry weight in air; D = polybag weight in air; C = weight of saturated sample and polybag in water; F = specific gravity of polybag at 25 °C.

Finally, total pores are determined using Eq. (3.5) as follows:

$$n = \frac{G_{mm} - G_{mb}}{G_{mm}} \quad (3.5)$$

3.5 LABORATORY PERMEABILITY TESTING

Florida apparatus was used for laboratory permeability measurement. It is repeatable, available, and easy to use. Flow in this permeameter is one-dimensional. It uses Eq. (2.3). Figure 3.6 shows the permeability test set-up in the laboratory. Both ends of the cored sample are smoothed using a wet saw. Before placing a sample in the laboratory permeameter, it was saturated using Corelok™ device. In Corelok™, a sample is vacuum sealed in a plastic bag, which is cut open under water to saturate the sample. This method has shown to be more effective than flask-vacuum saturation (Tarefder et al. 2002). Petroleum jelly is applied on the curve surface of the sample to make lateral surface impermeable and to have a good seal so that no water flow through the interface of sample and permeameter. The sample was then placed inside a cylinder enclosed by a membrane and pressurized to confine the side so that water flows in vertical direction only. Temperature of the water is recorded. Water level was recorded at different time interval.

3.6 MOISTURE DAMAGE TEST

Moisture damage is measured by the ratio of wet to dry sample's IDT. For dry conditioning, the dry sample was placed inside a Ziploc bag and placed under water at 25 °C (77 °F) for two hours. For wet conditioning, the AASHTO T 283 method and MIST devices were used.

3.6.1 AASHTO T 283 Wet Conditioning

In the AASHTO T 283 method, an asphalt core is saturated using a vibro-deairator device that applies vibration and suction simultaneously. After saturation, the sample is placed inside a moist Ziploc bag and placed in a refrigerator for 16 hours at -23 °C (0 °F) for freezing. The sample is thawed in a hot water bath at a temperature of 60 °C (140 °F) for 24 hours followed by two hours of conditioning at 25 °C (77 °F) (24). Thus, in the AASHTO T 283 conditioning process, water is forced to enter inside the sample during saturation and to increase in volume during freezing. The increased volume of water causes increased pressure inside the pores of the sample causing damage. Thawing by hot water for 24 hours also contributes to the softening of the binder, mastic and samples.

3.6.2 MIST Wet Conditioning

In this method, a core sample is placed inside the MIST chamber filled with water as shown in Figure 3.7. A bladder inside the watertight chamber is used to increase and decrease the chamber pressure. In this study, the chamber temperature was set at 60 °C (77 °F) with a chamber pressure of 40 psi. A total of 3500 cycles of pressure increase and release were applied to the cored samples. As the number of cycles increase, the air inside the sample is replaced gradually with water. At certain cycles of intervals, air bubbles are released through the opening of the top of the chamber lid. Water inside the pores is pressurized to cause damage in the cores. After completion of MIST conditioning, the sample is placed under water at room temperature for about 2 hours for further conditioning.

3.6.3 Tensile Strength Testing

Dry and wet conditioned samples are loaded diametrically to fail in tension as shown in Figure 20. The load is applied at 50 mm/min rate and the peak value of the load is recorded. The indirect tensile strength is calculated using Eq. (3.6):

$$IDT = \frac{20P}{\pi DL} \quad (3.6)$$

where IDT = indirect tensile strength (kPa); P = peak force needed to crack the sample diagonally, recorded from the compression testing device (Newton); D = diameter of the sample (cm); L = length of the sample (cm).

Tensile Strength Ratio (TSR) of wet to dry samples is calculated using Eq. (3.7):

$$TSR = \frac{IDT_{wet}}{IDT_{dry}} \quad (3.7)$$

where IDT_{wet} = Average IDT of three wet conditioned samples, IDT_{dry} = Average IDT of three dry conditioned samples.

Table 3.1 Participation of districts from NMDOT

District	Low Permeability/ Good performing Pavement	High Permeability / Bad performing Pavement
District 2 District 3	US 285 MP 115-MP 205 I-40 from Coors to Unser	US 70 MP 268 - MP 301 I-25 from south of Budaghers north to Santa Fe county line (District 3 boundary)
District 6	C.N. ESG5B66, US 491, M.P. 59.0 – 67.7, San Juan County C.N. G1436ER, I-40, M.P. 126.2 – 130.7, Cibola County	I-40 mile markers 18 – 22 C.N. 6100430, NM 264, M.P. 10.6 – 13.1, McKinley County, Roadway Rehab with WMA
Dist. 5	US 285, MP 284 – 290 NM 14, MP 47 - 50	US 84, MP 233 – 238 NM 344, NM 2 – 14

Table 3.2 Field permeability test locations

Pavements	Location
US285	MP126.23
	MP140.53
	MP152
	MP285.25
	MP285.5
US70	MP289.26
	MP282.2
	MP272.67
US491	MP60.9
	MP60.5
	MP60.7
I40	MP335.5
US264	MP10
MN14	MP46.80NB
	MP46.80SB
	MP46.9SB
NM344	MP1.80
	MP1.82
	MP1.84
US84	MP235.8
	MP235.9
	MP236
I40	MP23.1

Table 3.3 Selected pavements for laboratory testing

Good Performing Pavements (Not showing Moisture Damage)			Bad Performing pavements (Showing Moisture Damage)		
Pavement location	ID	Number of layers	Pavement location	ID	Number of layers
US285 MP126.3	1	2	US70 MP289.26	9	3
US285 MP285.25	2	3	US70 MP282.2	10	3
NM344 MP1.80	3	1	US70 MP272.67	11	3
NM14 MP46.8	4	3	NM264 MP10	12	1
US491 MP60.7	5	3	US491 MP60.9	13	3
US491 MP60.5	6	3	US285 MP140.53	14	2
NM14 MP46.9	7	3	NM344 MP1.82	15	1
NM344 MP1.84	8	2	I40 MP23.1	16	3



(a) Pavement marked to test permeability

(b) Field permeability testing

Figure 3.1 Field permeability test set up

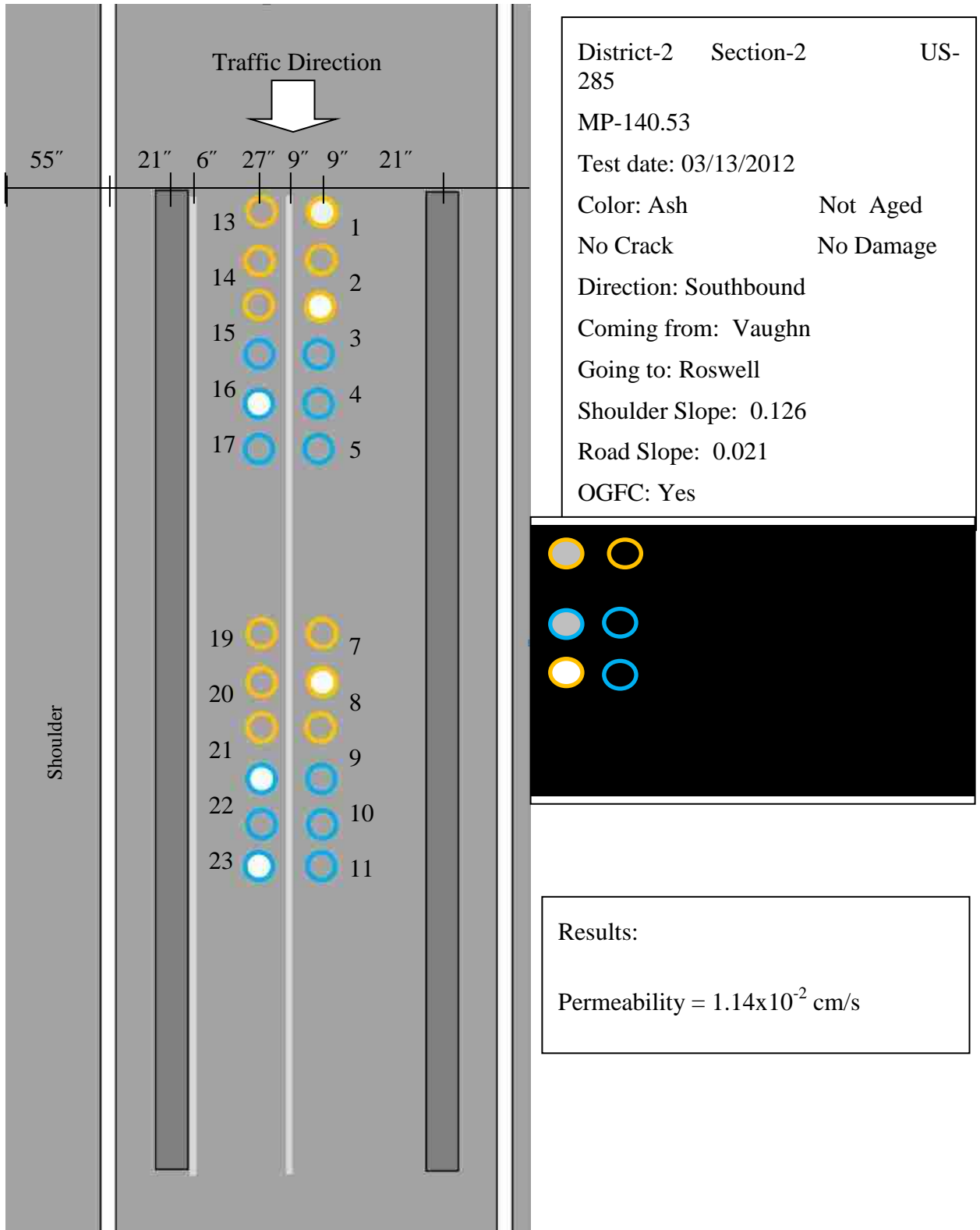


Figure 3.2 Field permeability test summary for US285 MP 140.53

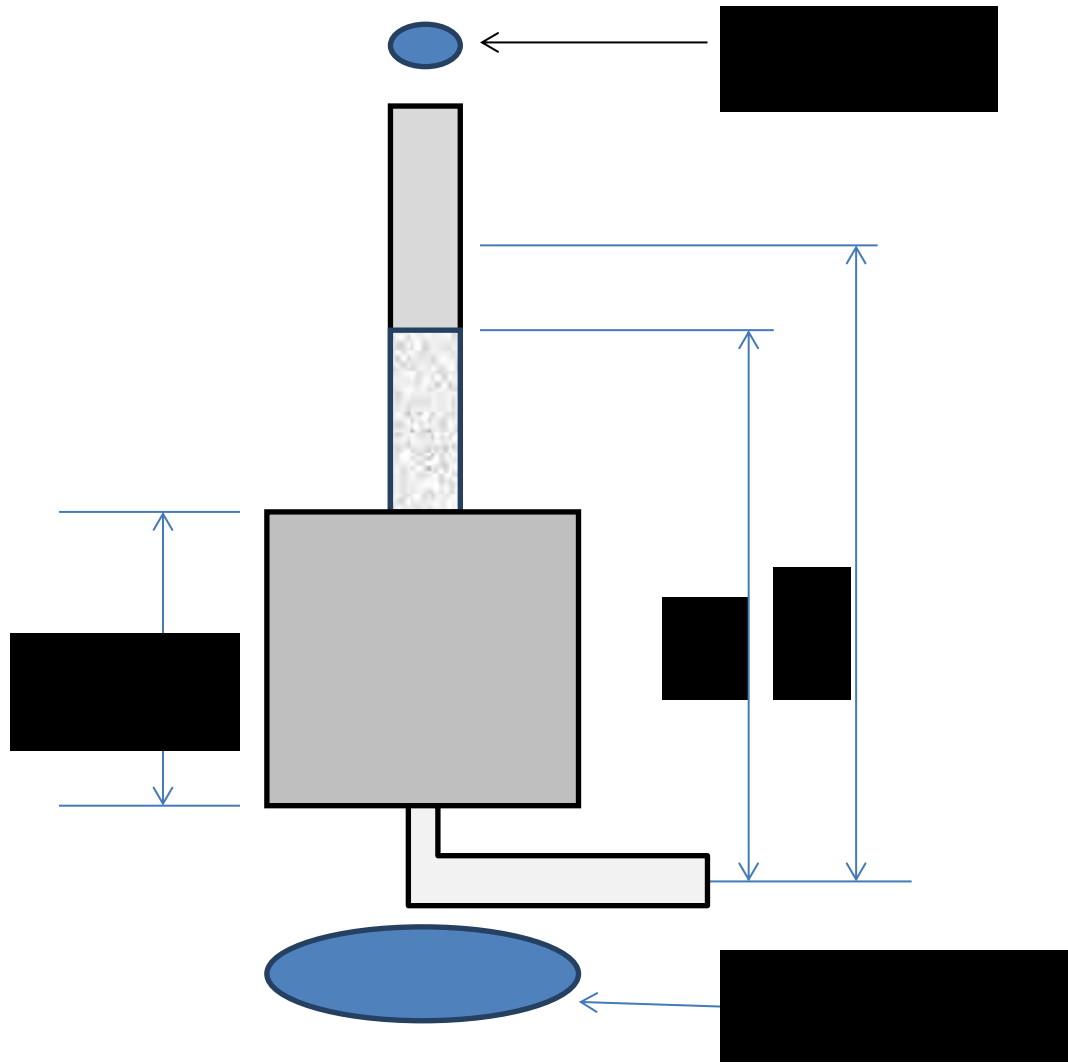


Figure 3.3 Schematic of falling head permeameter

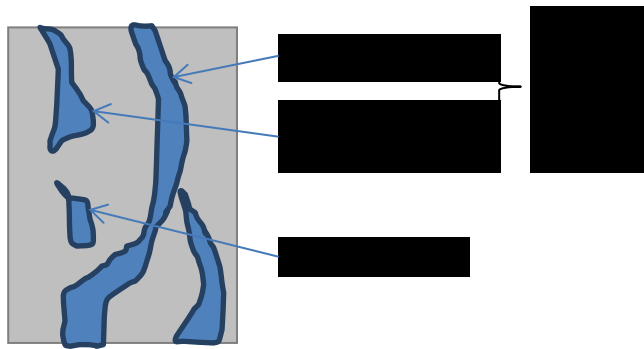


Figure 3.4 Different types of pores inside a HMA core sample



(a) Vacuum sealed sample inside a polybag (b) Weight of sealed sample under water

Figure 3.5 Bulk specific gravity of a cored sample



Figure 3.6 Laboratory permeability test



Figure 3.7 Sample in the MIST chamber



Figure 3.8 IDT testing in progress

CHAPTER 4

CORRELATING PERMEABILITY TO MOISTURE DAMAGE

4.1 INTRODUCTION

In this chapter, permeability is determined in the field at selected locations. Cores collected from these locations are tested for full depth permeability and permeability of samples cut into layers. The samples are then tested for moisture damage by the AASHTO T 283 and MIST procedures. Then comparison among different permeabilities and different moisture damage are made and analysis is conducted to see whether permeability is correlated to moisture damage. Permeability and moisture damage of laboratory compacted samples are also determined to see their correlation.

4.2 TEST MATRIX

The test matrix is shown in Table 4.1. A total of 15 field cores were collected from each pavement section. Six of them were used to determine full depth permeability and nine of them were separated into individual layers. As shown in Table 3.3, 10 of the 16 pavements have three layers, 3 of them have two layers, and 3 of them have a single layer. Therefore, the total number of layers after separation is $(10 \times 3 + 3 \times 2 + 3 \times 1) = 39$. Ideally, if each layer represents a different mix, permeability of the 39 mixes is evaluated in this study. A total of $39 \times 9 = 351$ cores were tested for permeability. One third of the samples ($351/3 = 117$ cores) were subjected to each of the dry, MIST and the AASHTO T 283 conditioning. It can be noted that no permeability test was conducted on MIST and the AASHTO conditioned samples. All permeability tests were conducted

using the Corelok Saturation method and then using the falling head permeability test method.

4.3 RESULTS AND DISCUSSIONS

Permeability is determined at three different modes (Field, full depth and layered samples). Moisture damage is also determined by three different procedures. Each of the permeability are tried to be correlated with each of the moisture damage. Also, different permeabilities and moisture damage are also compared. Permeability and moisture damage are also correlated with mix-volumetric.

4.3.1 Mix-volumetric

The Core samples were tested in the laboratory for bulk specific gravity (G_{mb}), maximum specific gravity of loose mix (G_{mm}), asphalt content (% AC) by ignition oven, total pores and gradation. Total pores vary from 6% to 10% and asphalt content varies from 4% to 7% as shown in Table 4.2. Mixes from all locations have 19 mm Nominal Maximum Size (NMAS) aggregate. The power charts are shown in Figure 4.1(a) to (d). Most of the mixes have 19 mm NMAS aggregate. Good performing sections have almost equal portion of power gradation curve above and below maximum density line. Bad performing sections have more portions below maximum density line. Therefore, good performing pavement sections contains more fine aggregates than bad performing pavement sections

Bad performing pavements maintain a regular “S” shape whereas for good performing pavements the lower portion of the curve become parallel to maximum density line. This

indicates, for good sections, the proportion of fine aggregates is equal to the proportion that produces maximum density.

4.3.2 Field Damage with Field Permeability

Individual and average field permeability values of pavement section 9 are shown in Table 4.3. Similar averaging is done for the other 15 pavement sections and is plotted in Figure 4.2. Figure 4.2(a) shows permeability of the good performing sections and Figure 4.2(b) shows permeability of the bad performing sections. It can be seen that average permeability of the eight good performing sections is 62.7×10^{-5} cm/s which is much less than the average permeability of the bad performing pavements, 298×10^{-5} cm/s. This was expected. However, from Figure 4.2(a), it can be seen that pavement 5 has higher permeability than 125×10^{-5} cm/s, which is the required limit set by many DOTs (Ahmad and Tarefder 2013). From Figure 4.2(b), permeability of some pavement sections are less than 125×10^{-5} cm/s because field permeability depends on lot of factors like, air voids of each layer, continuity of continuous air voids through different layers, track coat, seal coat, base permeability, flow direction, etc. As for the example, if any layer below the top layer is impermeable, the permeameter will measure only the lateral flow yielding less permeability. There may be a higher permeable layer, though, and more or less field permeability of the individual pavement is not related to visual stripping of the pavement. In general, pavements with higher field permeability exhibit higher field damage in most of the cases, but this is not true always.

4.3.3 Field Damage with Laboratory Permeability of Full Depth Samples

Individual and average laboratory permeability results of full depth samples of pavement section 9 are also shown in Table 4.3. Similarly, average permeability for all other pavement sections are determined and plotted in Figure 4.3. Figure 4.3(a) shows the full depth permeability of eight good performing pavement sections and Figure 4.3(b) shows the full depth permeability values for eight bad performing sections. It can be seen that the average permeability of the good performing sections is 4.15×10^{-5} cm/s, which is much lower than the average permeability of the bad performing sections (69.7×10^{-5} cm/s). This was expected. Because of the presence of the interface and the heterogeneous nature of the different layers, full depth permeability is very low and sometimes zero. However, one permeability value in Figure 4.3(a) is higher compared to other good performing sections. Also, permeability of some bad performing sections in Figure 4.3(b) is almost zero. This is unexpected. Therefore, pavements with higher full depth permeability undergo more *in-situ* damage with some exceptions.

4.3.4 Field Damage with Laboratory Permeability of Samples Separated into Layers

The permeability values for samples separated into the layers of section 9 are shown in Table 4.3. Similarly, average permeability values for all other pavement sections are shown in Figure 4.4. Figure 4.4(a) shows the permeability values for good performing sections and Figure 4.4(b) shows the permeability values for bad performing sections. The average of all permeability values for good performing sections is 22.9×10^{-5} cm/s, which is much lower than the average of all permeability values for bad performing sections (78.6×10^{-5} cm/s), as expected. All permeability values of good performing sections are less than 125×10^{-5} cm/s. Some permeability values of the bad performing

sections are less than 125×10^{-5} cm/s. For good performing sections, four top layer permeability values are almost zero. For other sections, the top layer has the highest and middle layer has the lowest permeability. Here, average permeability for, the top layer is 39×10^{-5} cm/s, for the middle layer is 18.8×10^{-5} cm/s, and for the bottom layer is 7.4×10^{-5} cm/s. Pavements with zero permeability of the top layer, water can't enter into the pavement, resulting in less interaction between the pavement and water and less damage. For higher top layer permeability, it acts as OGFC. It provides good drainage and less damage occurs. Most of the bad performing pavements have higher permeability values for all layers. The average permeability, for the top layer is 72.8×10^{-5} cm/s, for the middle layer is 97.3×10^{-5} cm/s, and for the bottom layer is 70.6×10^{-5} cm/s Here, water saturates the HMA and base very quickly after precipitation. This may damage the pavement severely due to the pumping action. Therefore, pavement with zero or higher top layer permeability compared to other layers exhibits less *in-situ* damage and pavement with high permeability to all layers exhibits more field damage.

4.3.5 MIST Damage with Permeability

The calculation for MIST TSR for pavement section 9 is shown in Table 4.4. Average TSR of all layers is determined to compare with field and laboratory full depth permeability. TSR for all other pavement sections are calculated similarly and plotted in Figure 4.5. Figure 4.5(a) shows the relation between MIST TSR and field permeability, Figure 4.5(b) shows the relation between MIST TSR and laboratory full depth permeability, and Figure 4.5(c) shows the correlation between MIST TSR and samples separated into layers. None of the figures show good correlation between TSR and permeability. This can be explained as follows. MIST cyclic pressure acts not only inside

the pore but also on the sides. When a less permeable sample is placed inside the MIST chamber at 60°C temperature with 40 psi pressure for 3500 cycles, it gets soft due to temperature and damaged due to cyclic pressure on the surfaces of the soft sample. Therefore, some samples show less permeability but more damage, which is unexpected. Therefore, MIST damage cannot be correlated with permeability.

4.3.6 AASHTO T 283 Damage with Permeability

The calculation for the AASHTO T 283 TSR for pavement section 9 is shown in Table 4.4. Average TSR of all the layers is determined to compare with field and laboratory full depth permeability.

TSR for all other sections are calculated similarly and plotted in Figure 4.6. Figure 4.6(a) shows the relation between the AASHTO T 283 TSR and field permeability, Figure 4.6(b) shows the relation between the AASHTO T 283 TSR and laboratory full depth permeability, and Figure 4.6(c) shows the correlation between the AASHTO T 283 TSR and samples separated into layers. In case of the AASHTO T 283, the increase of water volume in the voids due to freezing exerts internal pressure on the sample. The more permeable voids indicate that more water can get in. This eventually increases the internal pressure due to freezing and more damage occurs. Field permeability tests and permeability of full depth samples doesn't show any relation with damage, as shown in Figure 4.6(a) and Figure 4.6(b) respectively. From laboratory permeability tests on layered samples, a good correlation of TSR with permeability was obtained and is shown in Figure 4.6(c).

4.3.7 Laboratory and Field Permeability

Average permeability values of full depth samples, samples separated by layers and field results were compared for all roads and shown in Figure 4.7. In most cases, field permeability > top layer permeability > full depth permeability. In the field, water moves in all directions whereas in the lab, the flow is one-dimensional. For the full depth sample, the interface and discontinuity of interconnected voids between layers retards the flow. For a few locations, field permeability is less than lab permeability. In these locations, the middle and bottom layers are almost impermeable. This chokes the vertical flow. Hence, field permeability here is caused only by lateral flow. For the single layered sample, field and lab test gave almost identical result. Therefore, the full depth sample has the lowest and field permeability has the highest value. However, no correlation between them can be made.

4.3.8 MIST and AASHTO T 283 Damage

Figure 4.8 compares TSR values obtained by the AASHTO T 283 and MIST. MIST TSR values are higher than the AASHTO T 283 TSR for most of the samples. For a few samples, the AASHTO T 283 TSR is higher than MIST TSR. This can be explained as follows: MIST is independent of permeability and the AASHTO T 283 TSR increases with a decrease of permeability. Therefore, for the less permeable sample, it is possible that the AASHTO T 283 TSR will be more than MIST TSR.

4.3.9 Field Damage with Laboratory Damage

Figure 4.9 shows the TSR values for good and bad performing sections. Figure 4.9(a) and 4.9(b) are for the AASHTO T 283 conditioned samples and Figure 4.9(c) and 4.9(d) are

for MIST conditioned samples. All good performing sections are supposed to have TSR values more than equal to 0.8 and bad performing sections should have less. However, the results shows $TSR < 0.8$ for 11 good performing sections and $TSR > 0.8$ for 3 bad performing sections, in case of the AASHTO T 283. Similar scenario for MIST is observed. This is unexpected. This happens because; MIST and the AASHTO T 283 sometimes do wrong prediction. Permeable porosity might not be uniformly distributed all through the sample. If there is less porosity along the line of loading during IDT, higher TSR value might be obtained, although, higher damage at other location of the sample might occur. The opposite action is also possible. Therefore, MIST or the AASHTO T 283 method may not give accurate prediction of moisture susceptibility of HMA.

4.3.10 Laboratory Compacted Samples

Correlation between Permeability and Air Voids

The permeability and air void relations for laboratory and field compacted cores are shown in Figure 4.10(a) and (b) respectively. For laboratory compacted samples, permeability is zero for air voids $< 6.0\%$. However for field compacted samples, many sample with $< 6\%$ air voids have non zero permeability. Therefore, permeability characteristics of laboratory compacted cores are not comparable with field collected cores. The gyratory compactor may produce the similar dense sample as in the field, but cannot produce the same connectivity of voids as in the field. Thus, it is not feasible to use laboratory compacted samples to evaluate permeability characteristics of HMA pavements.

Permeability and Moisture Damage

Permeability and moisture damage relation for laboratory compacted samples are shown in Figure 4.11(a). None of the MIST or the AASHTO T 283 shows any good correlation with permeability. The AASHTO T 283 and MIST TSR values are compared in Figure 4.11(b). In case of field collected cores, MIST TSR values were always higher than the AASHTO T 283 TSR. For, laboratory compacted samples, these two TSR values are almost similar. A paired t-test yields a p value 0.45. That is, for laboratory compacted samples, the AASHTO T 283 and MIST cause same damage.

4.4 CONCLUSIONS

From this study, the following conclusion can be made,

- All kind of permeabilities (field, full depth and laboratory) are higher for good performing sections than bad performing sections. Therefore, permeability increases the potential of moisture damage. It is also observed that pavements with decreasing permeability from the top to the bottom layers exhibit less damage.
- The AASHTO T 283 TSR decreases with an increase of permeability and there exists a good correlation for laboratory testing on layered samples. Permeability doesn't affect MIST TSR. More damage occurs during the AASHTO T 283 conditioning than MIST conditioning with a few exceptions.
- Field permeability is higher than laboratory permeability in most of the cases. These two parameters cannot be correlated, as field permeability has a lot of variables.

Table 4.1 Test matrix

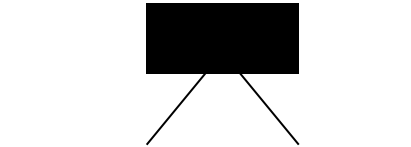

Pavement Sections	Permeability Testing	Moisture Conditioning	Cores (Laboratory Test)
8 good	Field Permeability	AASHTO T 283	
8 bad	Laboratory Permeability	MIST	

Table 4.2 Mix data for selected pavements

Pavement Sections	G _{mb}	G _{mm}	VA	AC	Pavement Sections	G _{mb}	G _{mm}	VA	AC
US285 MP 126.3TL	2.37	2.44	3.07	4.54	US70 MP272.67ML	2.22	2.45	9.25	4.04
US285 MP 126.3BL	2.19	2.37	7.60	4.93	US70 MP272.67BL	2.33	2.41	3.33	3.31
US285 MP285.25TL	2.41	2.58	6.39	6.13	NM264 MP10TL	2.32	2.47	6.05	4.61
US285 MP285.25ML	2.43	2.58	5.78	5.80	US285 MP140.53TL	2.27	2.47	8.10	6.40
US285 MP285.25BL	2.41	2.52	4.18	6.05	NM344 MP1.82TL	2.26	2.50	9.77	5.93
NM344 MP1.80TL	2.28	2.51	9.03	5.30	US285 MP152TL	2.25	2.45	7.88	5.94
NM14 MP46.8TL	2.28	2.49	8.30	5.60	US285 MP152ML	2.22	2.43	8.77	
NM14 MP46.8ML	2.33	2.44	4.42	5.50	US285 MP152BL	2.20	2.45	10.13	4.64
NM14 MP46.8BL	2.32	2.47	6.33	5.30	US491 MP60.5TL	2.21	2.47	10.36	5.42
US491 MP60.7TL	2.34	2.47	5.19	5.60	US491 MP60.5ML	2.31	2.44	5.29	5.50
US491 MP60.7ML	2.33	2.48	6.27	5.00	US491 MP60.5BL	2.31	2.44	5.29	5.51
US491 MP60.7BL	2.33	2.47	5.85	5.80	US491 MP60.9TL	2.33	2.46	5.35	5.51
NM344 MP1.84TL	2.31	2.46	6.10	4.63	US491 MP60.9ML	2.33	2.47	5.61	5.44
NM344 MP1.84BL	2.35	2.46	4.65	6.07	US491 MP60.9BL	2.34	2.44	4.02	5.63
US70 MP289.26TL	2.28	2.45	7.13	6.60	NM14 MP46.8SBTL	2.30	2.435	5.71	6.62
US70 MP289.26ML	2.23	2.46	9.29	6.99	NM14 MP46.8SBML	2.33	2.51	7.17	4.56
US70 MP289.26BL	2.22	2.45	9.23	7.13	NM14 MP46.8SBBL	2.29	2.47	7.39	5.79
US70 MP282.2TL	2.24	2.45	8.59	4.13	NM14 MP46.9SBTL	2.16	2.51	13.70	2.68
US70 MP282.2ML	2.21	2.46	10.30	4.10	NM14 MP46.9SBML	2.33	2.44	4.51	5.49
US70 MP282.2BL	2.29	2.43	5.97	4.52	NM14 MP46.9SBBL	2.33	2.46	5.12	6.55
US70 MP272.67TL	2.24	2.45	8.64	4.72	US285 MP140.53BL	2.08	2.39	12.97	5.67

Table 4.3 Permeability test results

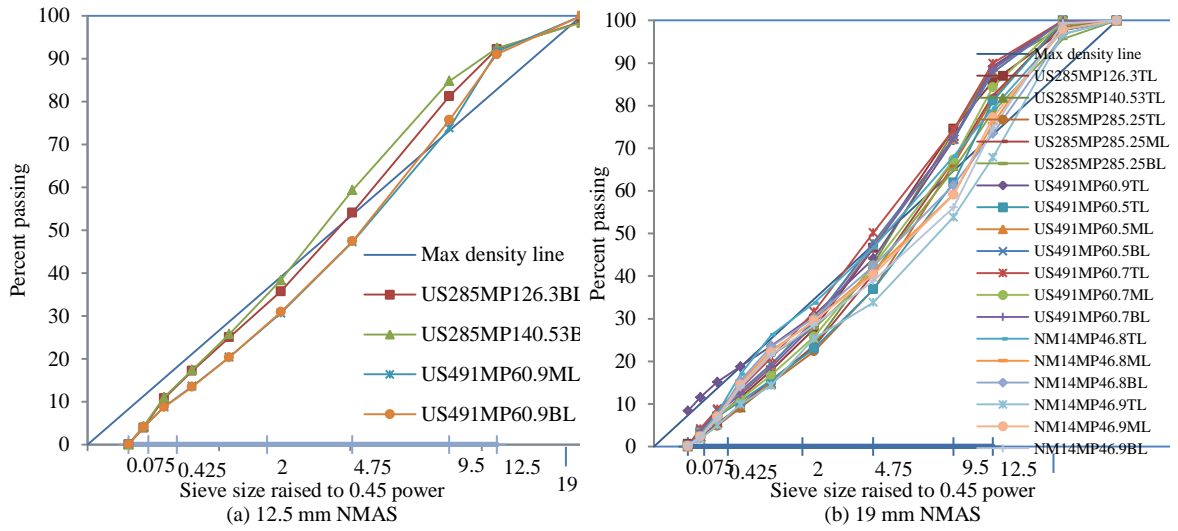
Field Permeability Tests					
Pavement Section	Test No	Permeability(cm/s)	Average	Standard Deviation	
9	1	48.1E-5	160.1E-5	92E-5	
	2	201.1E-5			
	3	92.4E-5			
	4	260.8E-5			
	5	100.4E-5			
	6	257.7E-5			
Laboratory Permeability of Full Depth Samples					
Pavement Section	Test No	Permeability(cm/s)	Average	Standard Deviation	
9	1	5.46E-06	5.38E-05	6.1E-5	
	2	7.22E-06			
	3	3.41E-06			
	4	1.35E-04			
	5	1.27E-04			
	6	4.54E-05			
Laboratory Permeability of Sample Cut into Layers					
Pavement Section	Layer	Test No	Permeability(cm/s)	Average	Standard Deviation
9	Top	1	5.2E-5	32.5E-5	19.3E-5
		2	13.6E-5		
		3	47.0E-5		
		4	31.6E-5		
		5	21.9E-5		
		6	58.6E-5		
		7	55.6E-5		
		8	17.1E-5		

		9	42.3E-5		
	Middle	1	37.2E-5	36.4E-5	0.5E-3
		2	57.6E-5		
		3	169.3E-5		
		4	3.9E-5		
		5	1.2E-5		
		6	0.7E-5		
		7	10.0E-5		
		8	44.0E-5		
		9	3.5E-5		
		Bottom	1		
	2		9.4E-5		
	3		66.7E-5		
	4		192.6E-5		
	5		383.2E-5		
	6		136.2E-5		
	7		3.6E-5		
	8		33.5E-5		
	9		11.2E-5		

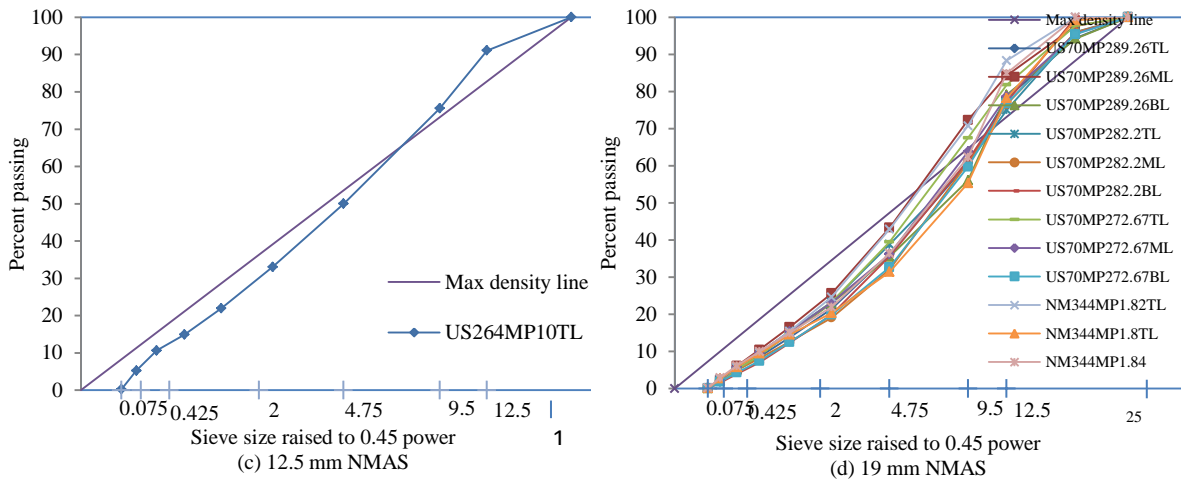
Table 4.4 TSR calculation

TSR Calculation for AASHTO T 283 Conditioned Samples									
Pavement Section		Dry Samples ID	IDT (psi)	Aver. IDT (psi)	T 283 samples ID	IDT (psi)	Ave. IDT (psi)	TSR	Ave.
9	Top layer	1	239.09	190.36	4	197.32	146.31	0.77	0.82
		2	175.68		5	115.70			
		3	156.33		6	125.92			
	Middle layer	1	189.31	189.23	4	141.41	132.66	0.7	
		2	185.44		5	138.20			
		3	193.93		6	118.39			
	Bottom layer	1	81.16	91.25	4	142.58	92.84	1	
		2	101.33		5	48.04			
		3	79.18		6	87.90			
TSR Calculation for MIST Conditioned Samples									
Pavement Section		Dry Samples ID	IDT (psi)	Average IDT (psi)	MIST samples ID	IDT (psi)	Ave. IDT (psi)	TSR	Ave.
9	Top layer	1	239.09	190.36	7	157.57	168.64	0.89	0.87
		2	175.68		8	166.31			
		3	156.33		9	182.03			
	Middle	1	189.31	189.23	7	109.01	135.12	0.71	

	layer	2	185.44		8	130.25		
		3	193.93		9	166.10		
	Bottom	1	81.16	91.25	7	85.01	91.07	1
	layer	2	101.33		8	93.90		
		3	79.18		9	94.32		



Good performing pavements



Bad performing pavements

Figure 4.1 Gradation curve for all pavement sections

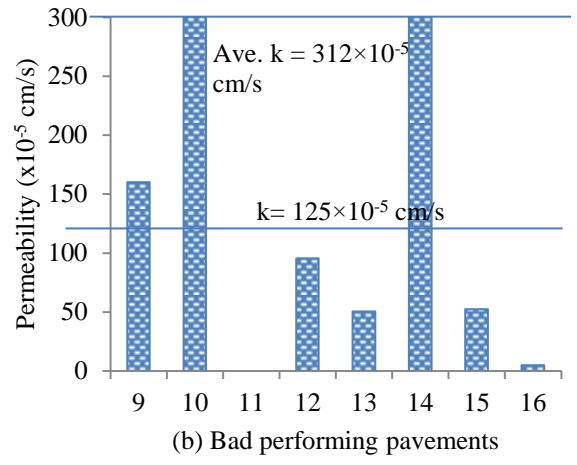
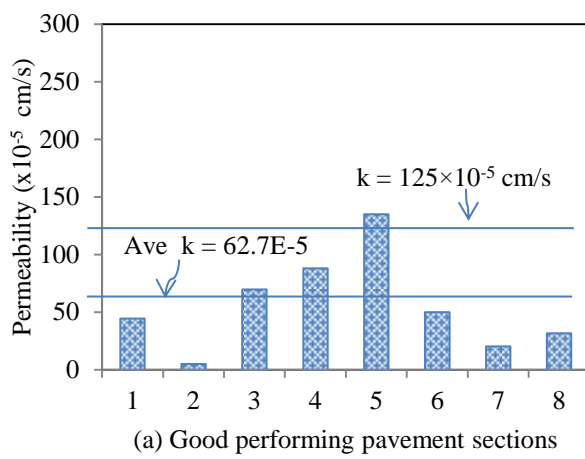


Figure 4.2 Field permeability at different damage conditions.

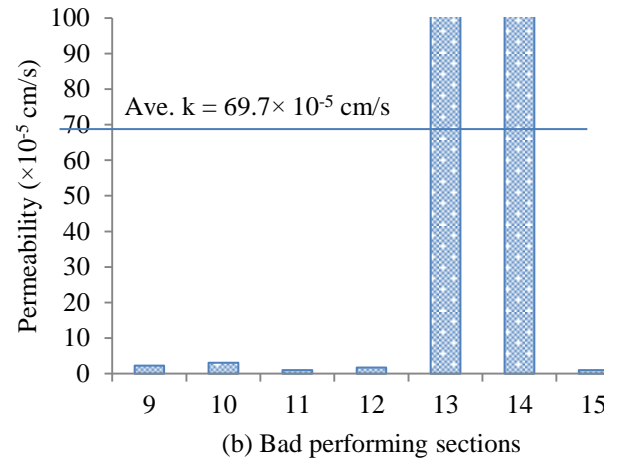
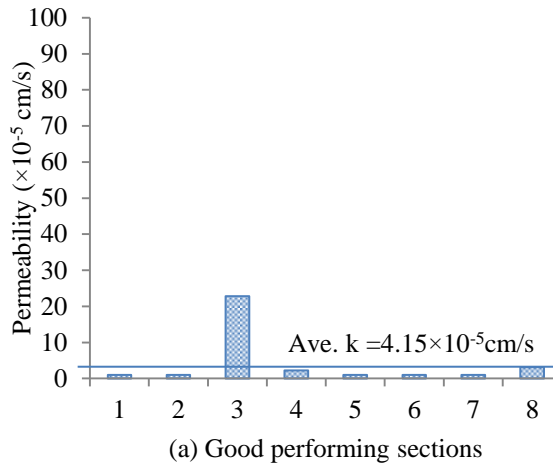
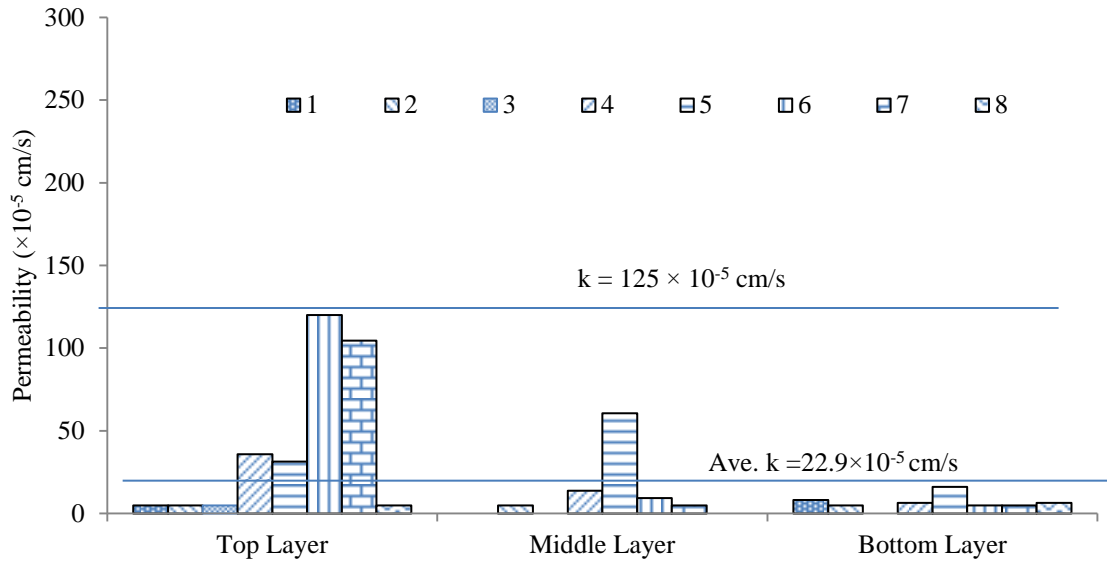
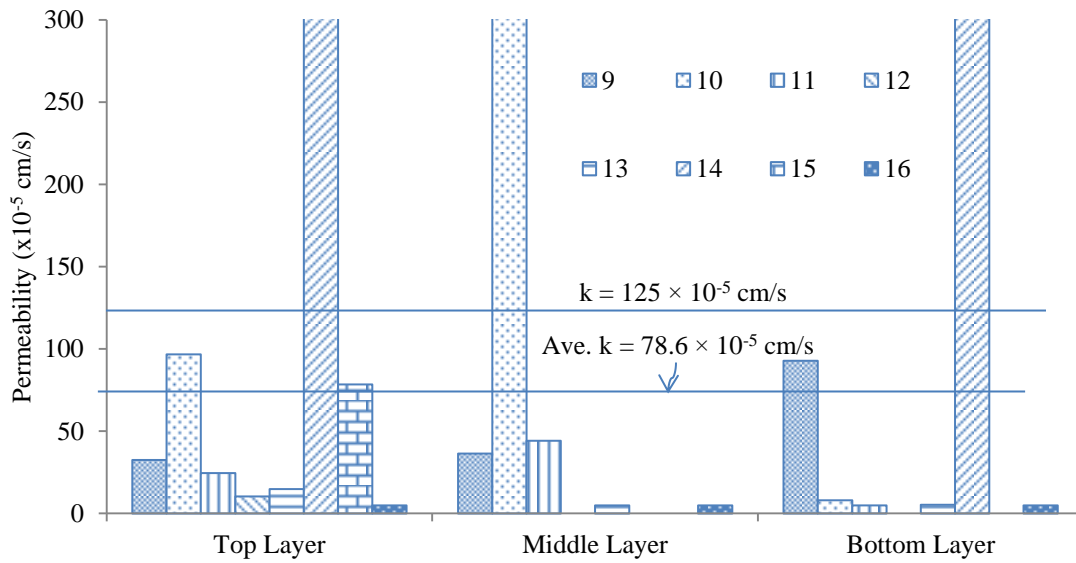


Figure 4.3 Laboratory full depth permeability at different damage conditions



(a) Different layers of good performing pavement section



(b) Different layers of bad performing sections

Figure 4.4 Laboratory permeability of separated samples at different damage conditions

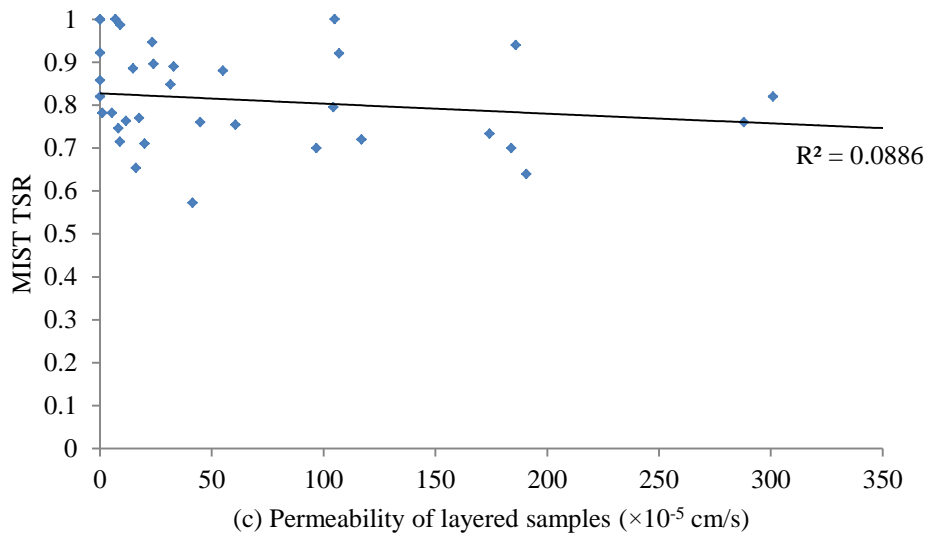
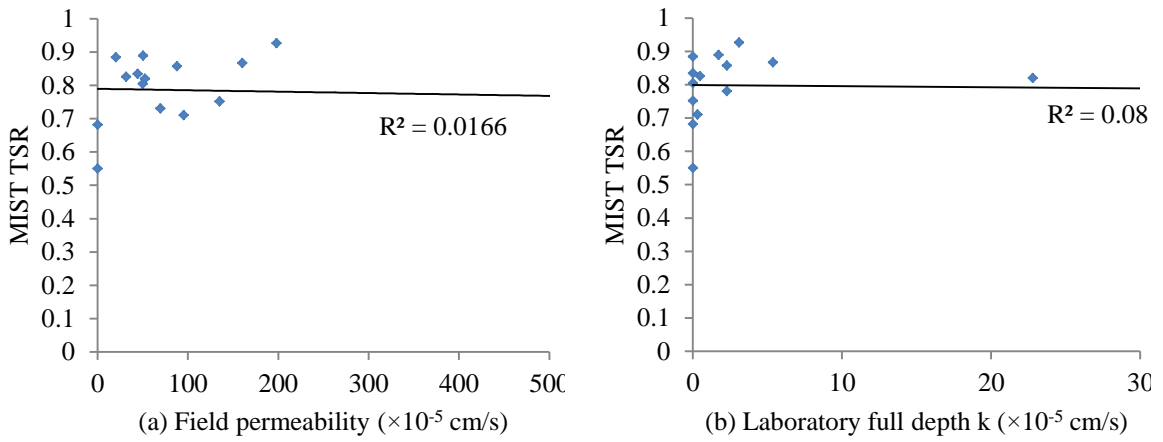


Figure 4.5 Correlation of MIST TSR and permeability at different modes.

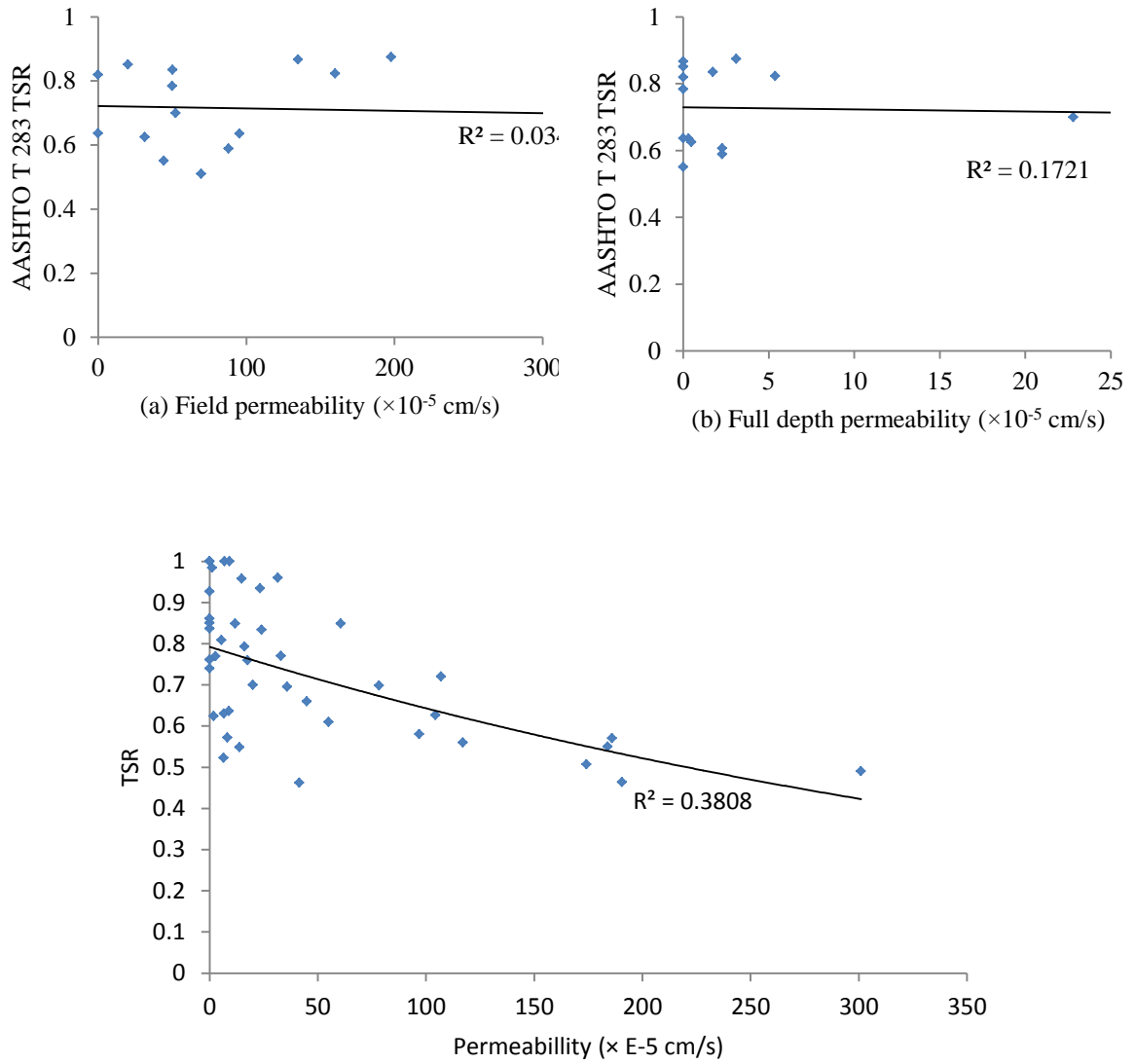


Figure 4.6 Correlation of AASHTO T 283 TSR and permeability at different test modes.

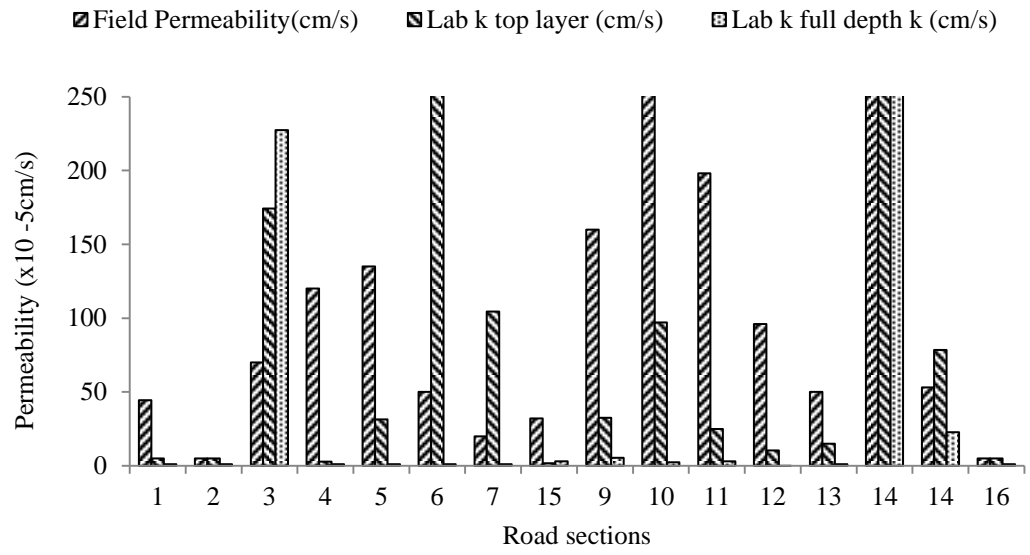


Figure 4.7 Permeability at different test modes

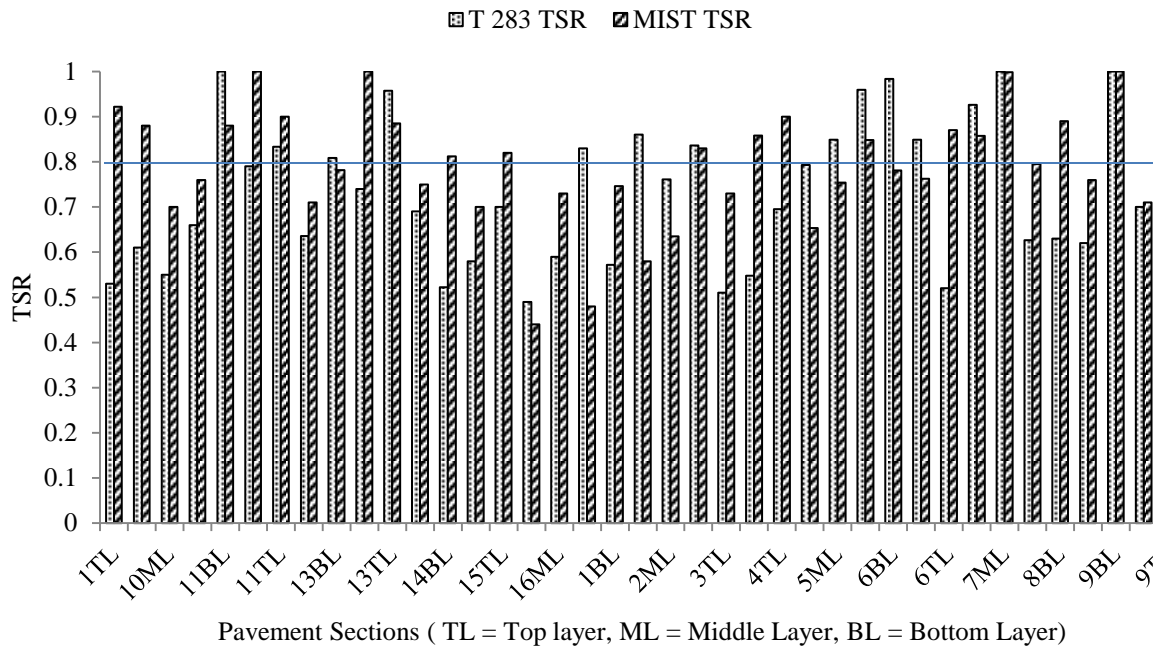
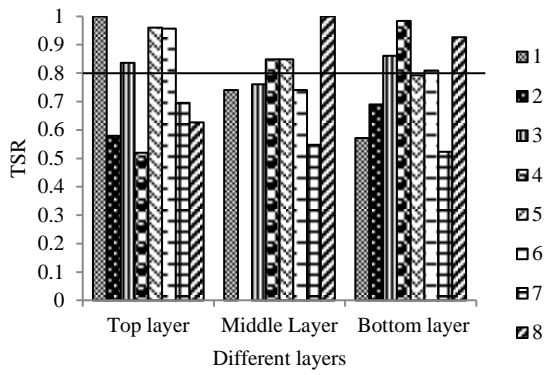
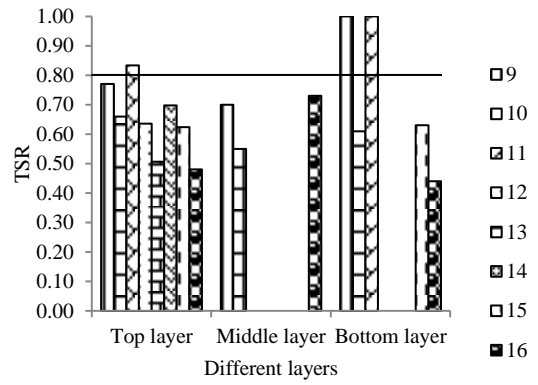


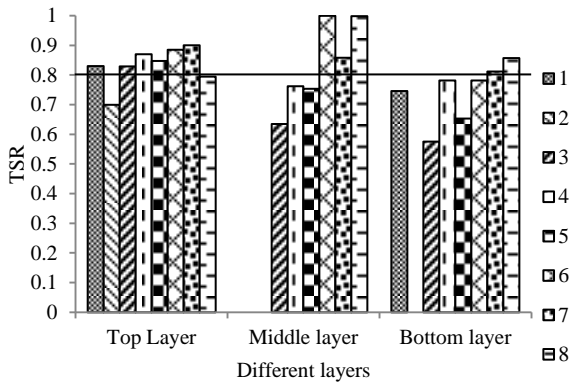
Figure 4.8 Comparisons between AASHTO T 283 and MIST TSR.



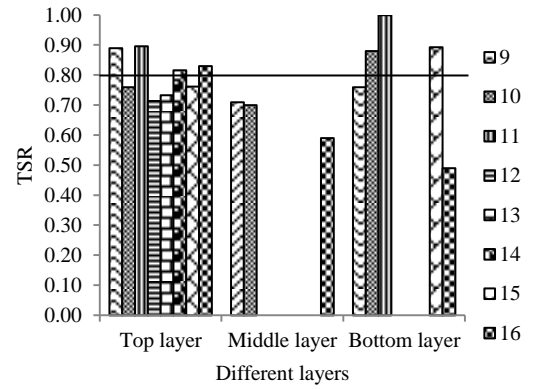
(a) AASHTO T 283 TSR for good performing sections



(b) AASHTO T 283 TSR for bad sections

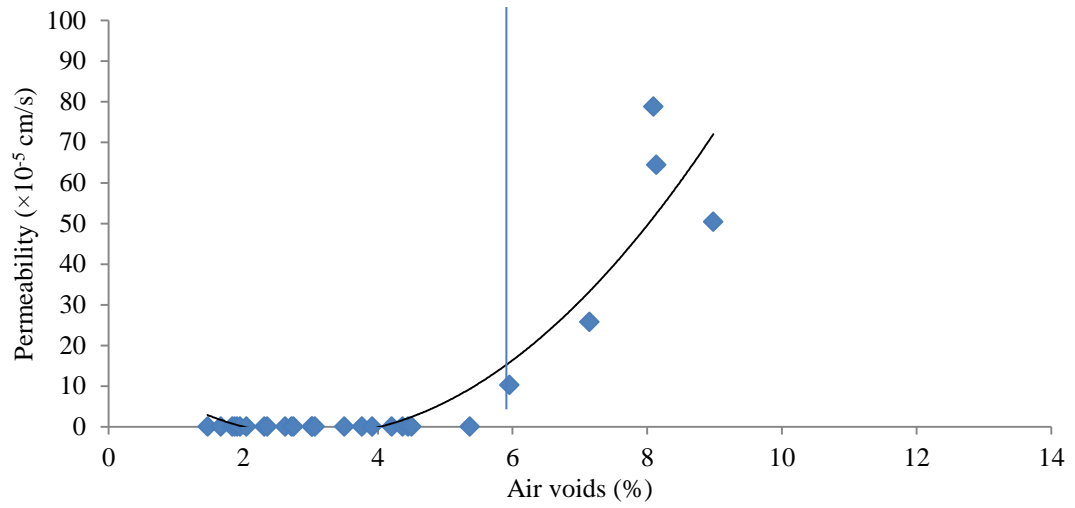


(c) MIST TSR for good pavement sections

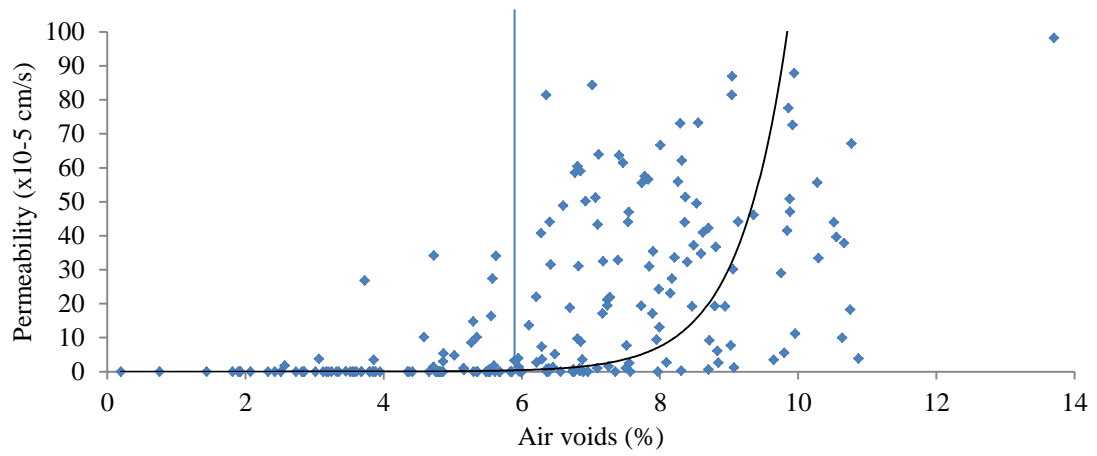


(d) MIST TSR for bad pavement sections

Figure 4.9 TSR values for good and bad performing pavement sections

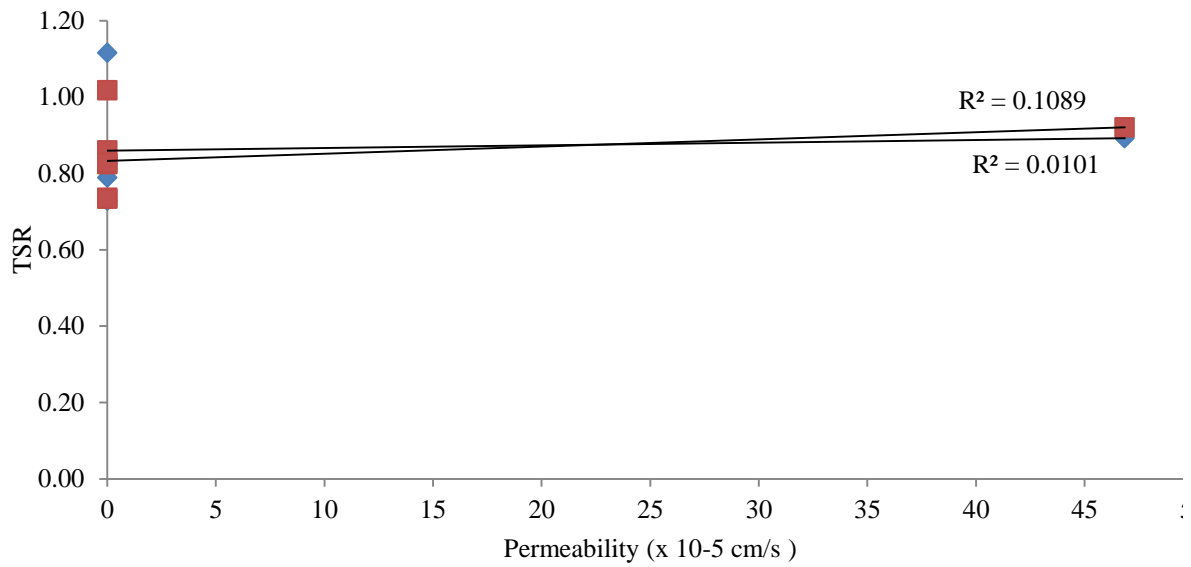


(a) Laboratory compacted samples

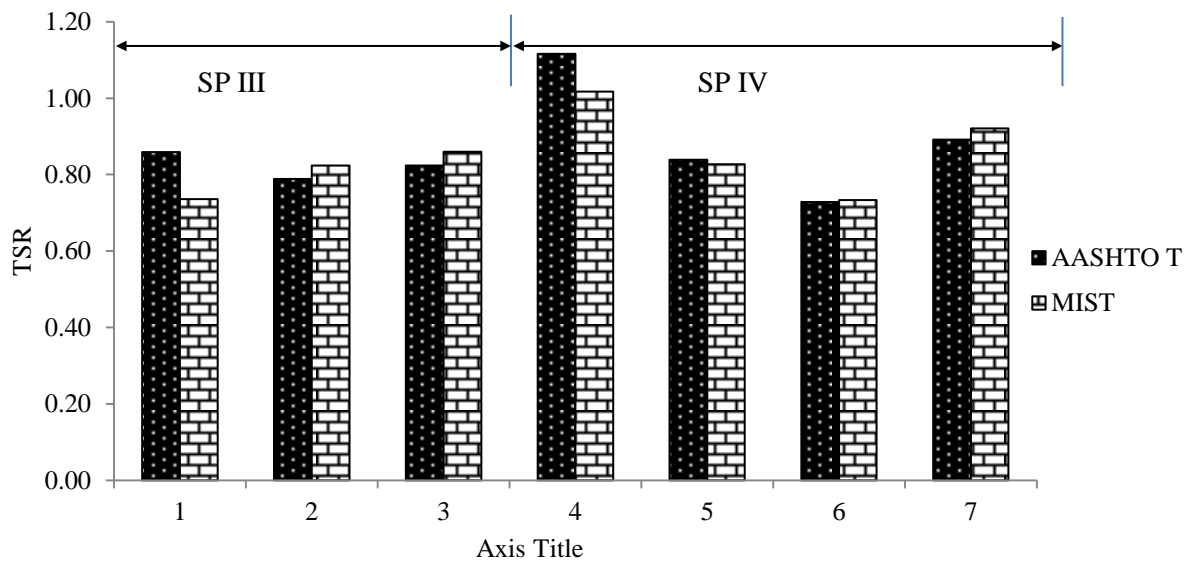


(b) Field cores

Figure 4.10 Permeability vs. air voids



(a) Permeability vs. TSR for laboratory compacted samples



(b) Comparison of AASHTO T 283 and MIST TSR for laboratory compacted samples

Figure 4.11 Permeability and moisture damage of labory compacted samples

CHAPTER 5

FIELD PERMEABILITY MODEL

5.1 INTRODUCTION

In this chapter, field permeability is determined by testing cored samples in the laboratory by two proposed models. The models are then verified by laboratory and field experiments. Initially, permeable pores of samples are determined in the laboratory using a conventional tracer method. Field permeable pores are determined using laboratory permeable pores and analytical method developed in this study. Finally, two models are proposed to determine field permeability using field permeable porosity.

Component of a pore in AC: permeable pores, dead-end pores and isolated pores are also measured correlated with the permeability and the moisture damage.

5.2 TRACER TEST

The laboratory setup for the tracer test is shown in Figure 5.1. Essentially, a salt concentration-measuring meter was added to a falling head permeameter. Before placing a sample in the laboratory permeameter, it was saturated using Corelok™ device. The sample was then placed inside a cylinder enclosed by a membrane and pressurized to confine the side so that water flows in vertical direction only. Salt water of a known concentration was poured inside the standpipe. The salt concentration of outflow was measured using a salt concentration meter. Constant head was maintained by continuously pouring water at inflow and discharge was measured. Darcy's velocity is determined using Eq. (5.1) and permeability is determined using Eq. (5.2):

$$q = \frac{Q}{A} \quad (5.1)$$

$$k_l = \frac{qL}{h} = \frac{QL}{Ah} \quad (5.2)$$

where q = Darcy's velocity, cm/s; Q = discharge rate, cm³/s; A = cross sectional area of the sample, cm²; k_l = laboratory permeability, L = length of the sample, cm; h = head, cm. For the one-dimensional tracer, the outflow concentration was determined by Eq. (5.3) (Stephen et al.1998):

$$\frac{C}{C_0} = \frac{1}{2} \left[1 \pm \operatorname{erf} \left(\frac{L - vt}{2\sqrt{Dt}} \right) \right] \quad (5.3)$$

where erf = an error function; c = outflow salt concentration, %; c_0 = inflow salt concentration, %; v = mean velocity of the tracer, cm/s; D = dispersion coefficient, cm²/s; and t = time, s. $C/C_0 = 0.5$ occurred when one pore volume of solution passed through the sample. The time required for $C/C_0 = 0.5$ is known as break through time, t_b . Laboratory permeable pores (n_{pl}) can be calculated from Eq. (5.4) (Jury and Horton 2004):

$$n_{pl} = \frac{t_b Q}{AL} \quad (5.4)$$

Numerical Example 1:

For a core sample collected from New Mexico Highway 344 (NM344) (MP1.80), the output from the salt concentration meter is shown in Figure 3.2. Salt concentration ratio C/C_0 is plotted against time. Ratio increases as time passes. Data is fitted to a sigmoidal 'S' shape curve. Breakthrough time from the graph can be found to be 58 s. The

measured Q is $0.645 \text{ cm}^3/\text{s}$. Sample diameter, length and constant head are 14.2 cm, 8.1 cm, and 53.5 cm, respectively. Thus, plugging these values in Eq. (5.2) and Eq. (5.4):

$$k_l = \frac{QL}{Ah} = \frac{0.645 \times 8.1}{158 \times 53.5} = 61.8 \times 10^{-5} \text{ cm/s}$$

and,

$$n_{pl} = \frac{t_b Q}{AL} = \frac{58 \times 0.645}{158 \times 8.1} = 2.915\%$$

5.3 FIELD PERMEABILITY MODEL

Total pores in an asphalt concrete sample can be divided in eight broad categories as shown in Figure 5.3(a). They are: a = pores that continue from top to bottom, b = dead-end pores at the top of the sample, c = pores that continue from top to side, d = pores that continue from bottom to side, e = dead-end pores at the bottom, f = pores that continue from side to side, g = dead-end pores at the side, and h = isolated pores.

When one-dimensional permeability test is performed on such sample (Figure 5.3(a)), water flow occurs because of pores shown as “ a ”, that is, the pores that continue from top to bottom of the sample. In the field, a fraction of “ c ” contributes to the flow through lateral flow. Therefore, permeable pores responsible for flow in the field are:

$$n_{pf} = a + f(c) \tag{5.5}$$

where n_{pf} = field permeable pores.

Assuming a field core with radius r has some permeable pores (a and c) at the top surface and they are distributed uniformly. If β = is the percent of curve surface pores that travel to top. Then, pores (A_l) that continue from the side to the top of the sample can be determined using Eq. (5.6):

$$A_l = 2\pi r L \beta \quad (5.6)$$

where L is the sample length. Therefore, pores responsible for vertical flow (A_{pl}) can be determined by the following Eq. (5.7):

$$A_{pl} = \pi r^2 \alpha - 2\pi r L \beta \quad (5.7)$$

where α = percent of the surface top area occupied by c and a pores, $\pi r^2 \alpha$ = flow area through c and a pores. In volumetric unit (dividing Eq. (5.7) by πr^2), laboratory permeable pores are:

$$n_{pl} = \alpha - \frac{2\gamma}{r} \quad (5.8)$$

where n_{pl} = laboratory permeable pores and $\gamma = L\beta$, a factor. Solving Eq. (5.8) for two different sample sizes yields:

$$\alpha = \frac{r_1 n_{pl1} - r_2 n_{pl2}}{r_1 - r_2} \quad (5.9)$$

$$\gamma = \frac{(n_{pl1} - n_{pl2})r_1 r_2}{2(r_1 - r_2)} \quad (5.10)$$

Hall and Ng (2001) have shown that the intensity of pores that continues from the side to the top of the sample is not uniformly distributed on the side. The intensity is higher near the top than the bottom. In this study, a triangular distribution of pore intensity may be assumed on the side of the sample (Figure 5.3(b)). In addition, β -pores near the top of the sample are less likely to continue to the bottom of the sample. In other words, β -pores near the top have small contribution to permeability. Therefore, permeable pore intensity can be assumed to be minimum (0.0) at the top and maximum (1.0) at the bottom. This distribution is shown in Figure 5.3(b) schematically.

For a differential length dy as shown in Figure 5.3(b), lateral pores that continue from side to top can be expressed as:

$$dA_l = \left[\frac{4\pi r \beta}{L} \times y \right] dy \quad (5.11)$$

Probability of these pores to continue to the bottom is:

$$p = \frac{1}{L}(L - y) \quad (5.12)$$

Therefore, part of dA_l that is permeable pores in case of field testing is:

$$dA_l^p = \frac{1}{L}(L - y) \times \left[\frac{4\pi r \beta}{L} \times y \right] dy \quad (5.13)$$

Integration of Eq. (5.13) yields the total portion of the lateral pores that continues from the top to the bottom and given below:

$$A_l^p = \frac{2}{3}\pi r(\beta L) = \frac{2}{3}\pi r \gamma \quad (5.14)$$

Therefore, the total permeable pores are (adding Eq. (5.7) with Eq. (5.14)):

$$A_p = A_{pl} + A_l^p = \pi r^2 \alpha - 2\pi r \gamma + \frac{2}{3}\pi r \gamma = \pi r^2 \alpha - \frac{4}{3}\pi r \gamma \quad (5.15)$$

In the volumetric unit:

$$n_{pf} = \alpha - \frac{4\gamma}{3r} \quad (5.16)$$

where n_{pf} = field permeable pores, γ and r were defined previously.

Model 1:

Assuming permeability increases exponentially (with base e and permeable pores as exponent), it can be written:

$$k \propto e^{m \times n_p} \quad (5.17)$$

where m is a constant and n_p is permeable pores. m is determined by solving Eq. (5.17)

for two different sample sizes as follows:

$$\frac{k_{l1}}{k_{l2}} = \frac{e^{m \times n_{pl1}}}{e^{m \times n_{pl2}}}$$

$$m = \frac{1}{n_{pl1} - n_{pl2}} \ln \frac{k_{l1}}{k_{l2}} \quad (5.18)$$

where k_{l1} = laboratory measured permeability of 6 in. diameter sample, k_{l2} = laboratory measured permeability of 4 in. diameter sample cored from the 6 in. diameter sample, n_{pl1} = laboratory measured permeable pores of 6 in. diameter sample, and n_{pl2} = laboratory measured permeable pores of 4 in. diameter sample cored from the 6 in. diameter sample.

Finally, field permeability (k_f) can be predicted using Eq. (5.19):

$$\frac{k_f}{k_l} = \frac{e^{m \times n_{pf}}}{e^{m \times n_{pl}}}$$

$$k_f = e^{m(n_{pf} - n_{pl})} k_l \quad (5.19)$$

Model 2:

Assuming permeability varies exponentially (with permeable pores as base):

$$k \propto n_p^\mu \quad (5.20)$$

where μ is a constant and n_p was defined before. μ is determined by solving Eq. (5.20)

for two different sample sizes as follows:

$$\frac{k_{l1}}{k_{l2}} = \frac{n_{pl1}^\mu}{n_{pl2}^\mu}$$

$$\mu = \frac{\ln\left(\frac{k_{l1}}{k_{l2}}\right)}{\ln\left(\frac{n_{pl1}}{n_{pl2}}\right)} \quad (5.21)$$

All parameters were defined before. Finally, field permeability (k_f) can be predicted by solving Eq. (5.20) for field and laboratory permeability and permeable pores:

$$\frac{k_f}{k_l} = \frac{n_{pf}^\mu}{n_{pl}^\mu}$$

$$k_f = \left(\frac{n_{pf}}{n_{pl}} \right)^\mu k_l \quad (5.22)$$

Numerical Example 2

For a sample from NM344 MP1.80:

For a sample of radius $r_1 = 7.05$ cm, $k_{l1} = 61.8 \times 10^{-5} \frac{cm}{s}$ and $n_{pl1} = 2.915\%$ (as the procedure described in *Numerical Example 1*)

For a sample of radius $r_2 = 5$ cm cored from previous sample, $k_{l2} = 47.4 \times 10^{-5} \frac{cm}{s}$ and $n_{pl2} = 2.086\%$ (as the procedure described in *Numerical Example 1*)

Using Eq. (5.9) and (5.10):

$$\alpha = \frac{r_1 n_{pl1} - r_2 n_{pl2}}{r_1 - r_2} = \frac{(7.05 \times 2.915 - 5 \times 2.086)}{7.05 - 5} = 4.94\%$$

$$\gamma = \frac{(n_{pl1} - n_{pl2}) r_1 r_2}{2(r_1 - r_2)} = \frac{(2.915 - 2.086) \times 7.05 \times 5}{2(7.05 - 5)} = 7.125$$

Using Eq. (5.16), field permeable pores is:

$$n_{pf} = \alpha - \frac{4\gamma}{3r} = 4.94 - \frac{4 \times 7.125}{3 \times 7.05} = 3.59\%$$

Model 1:

The constant m is calculated using Eq. (5.18):

$$m = \frac{1}{n_{pl1} - n_{pl2}} \ln \frac{k_{l1}}{k_{l2}} = \frac{1}{2.915 - 2.086} \ln \left(\frac{61.8}{47.4} \right) = 0.32$$

Therefore, field permeability can be predicted from Eq. (5.19):

$$k_f = e^{m(n_{pf} - n_{pl})} k_l = e^{0.32(3.59 - 2.915)} \times 61.8 \times 10^{-5} = 76.7 \times 10^{-5} \text{ cm/s}$$

Model 2:

The quantity μ can be calculated from Eq. (5.21):

$$\mu = \frac{\ln\left(\frac{k_{l1}}{k_{l2}}\right)}{\ln\left(\frac{n_{pl1}}{n_{pl2}}\right)} = \frac{\ln\left(\frac{61.8}{47.4}\right)}{\ln\left(\frac{2.915}{2.086}\right)} = 0.793$$

Using Eq. (5.22):

$$k_f = \left(\frac{n_{pf}}{n_{pl}}\right)^\mu k_l = \left(\frac{3.59}{2.915}\right)^{0.793} 61.8 \times 10^{-5} = 72.9 \times 10^{-5} \text{ cm/s}$$

Tests on two more samples were performed and average permeability of three of the samples was predicted as 391.5×10^{-5} cm/s which is much more than field permeability determined on that location (69.7×10^{-5} cm/s). Laboratory permeability for this location is 210.2×10^{-5} cm/s. Therefore, field permeability measurement gives unsatisfactory and predicted permeability yields a satisfactory result. Detailed discussion will be introduced in later section.

5.4 SELECTION OF CANDIDATE PAVEMENT

For moisture damage and permeability analysis, sixteen pavements were used. Among them, nine pavement sections have high permeability. For tracer test, the sample needs to be permeable. Therefore, the permeable nine pavement sections shown in Table 9 were used for tracer test and further analysis.

5.5 RESULTS AND DISCUSSION

5.5.1 Different Pores and Their Correlation with Permeability

For each location, three samples were tested for permeable pores (n_{pl}) in the laboratory using the tracer method. Average value of the three samples were determined and

correlated to effective pores (n_e) and total pores (n). As shown in Figure 5.4(a), the solid line represents the correlation between permeable pores and total pores and the dotted line represents the correlation between permeable pores and effective pores. Overall, n_{pl} doesn't show good correlation with n , because total pores contain isolated and dead-end pores. The relationship between n_{pl} and n_e is pretty good as n_e doesn't include isolated pores. The two regression lines are almost parallel as shown in Figure 35(a). That is, the rate of increase of n_{pl} with total pore and effective pores are the same.

Figure 5.4(b) shows that there is a good linear relation between n_{pl1} and n_{pl2} . The dotted line in this figure indicates $n_{pl1} = n_{pl2}$ (equal line). All points lay below the equal line indicating $n_{pl1} > n_{pl2}$. The regression line never intersects the equal line. This indicates whatever value n_{pl1} or n_{pl2} could have, they are not equal. These samples are identical but have a different radius. It means their permeable pores vary in the radial direction.

Figure 5.5(a) shows correlation of permeability with total pores (n), effective pores (n_e) and permeable pores (n_p). Permeability shows very poor correlation with total pores as it includes isolated and dead-end pores, which has no contribution to flow. Effective pores show a better correlation with permeability. As permeability is directly controlled by permeable pores, the correlation between permeability and permeable pores is pretty good.

Figure 5.5(b) describes the correlation between laboratory permeability (k_l) with predicted field permeability (k_f) (both of the models yield very close results, therefore only model 1 is used for further discussion). This will reduce the efforts needed for coring and measuring of n_p .

The measured permeable pore is less than effective pore and maintains a good correlation with effective pore and permeability. Therefore it can be concluded that, the tracer method gives a reasonable measurement of permeable pores of HMA.

5.5.2 Laboratory, Predicted and Field Measured Permeability

Figure 5.6 compares laboratory permeability, predicted permeability and field permeability. Field tests on the first four sections were performed on the driving lane, which was overlaid by an OGFC layer. Tests on the rest of the pavements were done on the shoulders without having any OGFC. As expected, measured field permeability results on the first four pavements are higher than the predicted permeability. For the other five pavements, field permeability results are lower compared to the predicted permeability. Measured field permeability values don't show any regular relationship with laboratory permeability, but predicted permeability does. Therefore, it can be stated that the permeability estimation from the newly developed theory gives better prediction of the field permeability of the compacted mix than.

To accommodate the field conditions (OGFC, coats etc.) a shift factor may be used with predicted permeability to make it equal to measured permeability. For pavements with OGFC, the ratio of measured to predicted permeability varies to a range of 4 to 22. Therefore, measured and predicted permeability cannot be correlated in this case. For pavements without OGFC, the ratio varies to a narrow range of 0.12 to 0.22 with an average of 0.17. A regression analysis on predicted and measure value by Anova gives an intercept of 9.43×10^{-5} cm/s with slope 0.132. The R^2 value in this case 0.95 which is pretty good. Finally, modified permeability is predicted using this regression analysis and

shown in Figure 5.6. The mean of error and standard deviation of error are 12.3% and 6.4% which are pretty good.

5.5.3 Quantification of Different Types of Pores and Their Relation with Moisture Damage

Figure 5.7(a) compares isolated, permeable and dead-end pores of the nine pavement sections. In all cases, permeable pores are higher than the other two types. Permeable pores drain out water. Hence, it reduces the ‘moisture damage due to pumping action’. On the other hand, dead-end pores hold the water for a long time after precipitation. Therefore, it has greater impact on moisture damage due to the pumping action. Isolated pores have no contribution on moisture or moisture related damage. Figure 5.7(b) shows the correlation of TSR (indication of moisture damage) with permeable pores and dead-end pores. As expected, moisture damage increases with the increase of dead-end pores and decreases with the increase of permeable pores. In all cases, the MIST line is above the AASHTO T 283 line, indicating less damage during MIST conditioning. The correlations in Figure 5.7(b) are not good as other factors like binder grade, aggregate type etc. was not considered during this study.

5.6 CONCLUSIONS

The following conclusions can be made from this study:

- Combination of a permeameter with a salt meter can be used to determine permeable pores of AC samples. Asphalt concrete sample’s permeability varies in radial direction due to increase in permeable pore in radial direction. Tracer method gives a reasonable measurement of permeable pores of AC samples.

- Permeability shows a good relationship with permeable pores. The analytical model developed in this study estimates field permeability of a HMA sample tested in the laboratory reasonably well.
- Pavement with more permeable pores is less susceptible to moisture damage. Pavement with more dead-end pores is more susceptible to moisture damage.

Table 5.1 Pavement sections selected for tracer test

Pavement Sections	Number of layer used (Top to bottom)
US285 MP140.53	1
US70 MP289.26	2
US70 MP 282.2	2
US70 MP272.67	2
US491 MP60.5	1
NM14 MP46.9	1
NM344 MP1.8	1
NM344 MP1.82	1
NM344 MP1.84	1



Figure 5.1 Permeable pores and permeability set up.

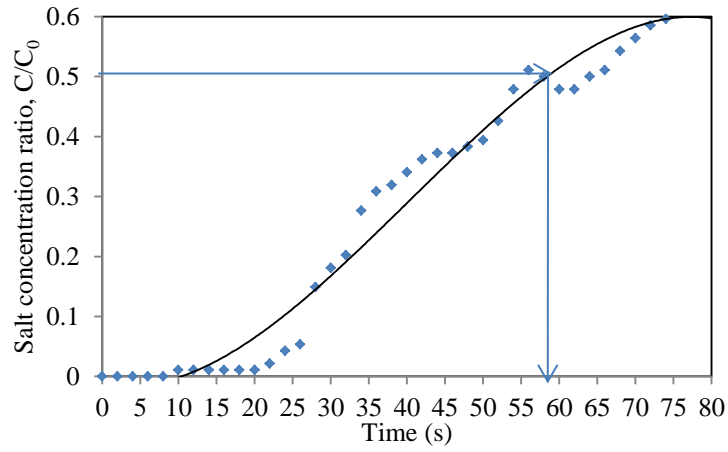
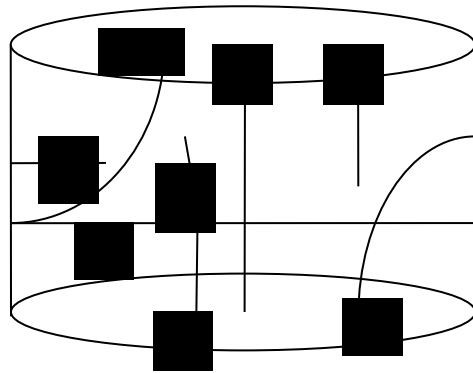
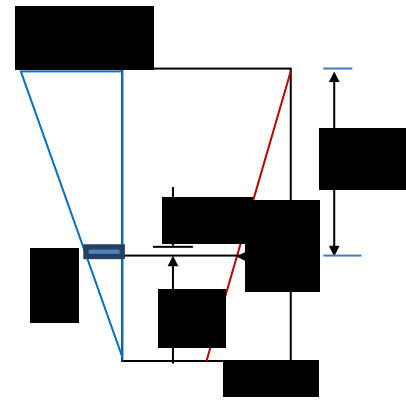


Figure 5.2 Breakthrough curve for a sample from NM344 at MP1.8.

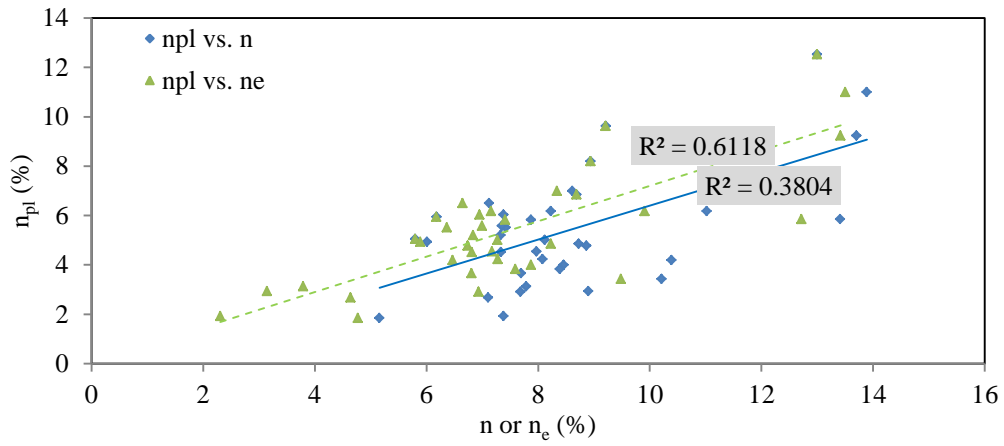


(a) Pores distribution inside a cored sample

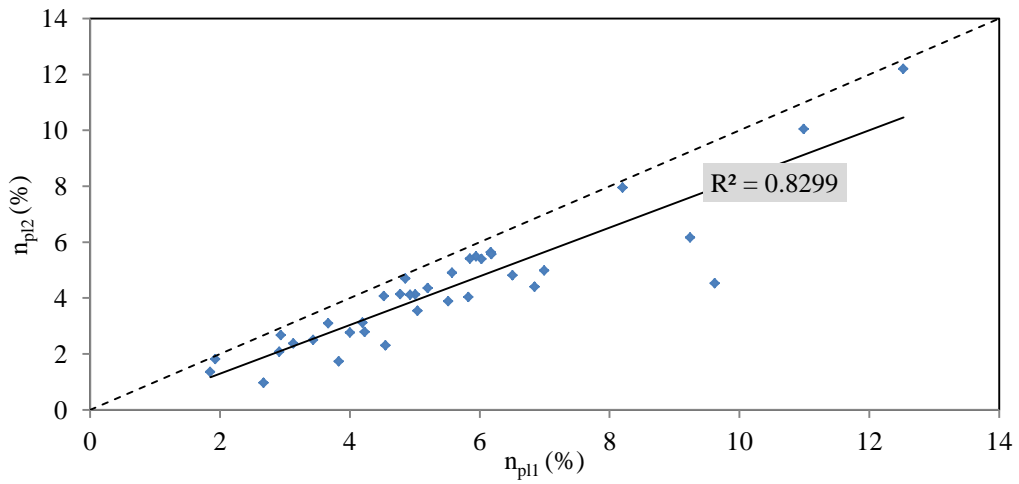


(b) β (left triangle) and the probability distribution (right triangle) on the side of the sample.

Figure 5.3 Different types of pores in a sample.

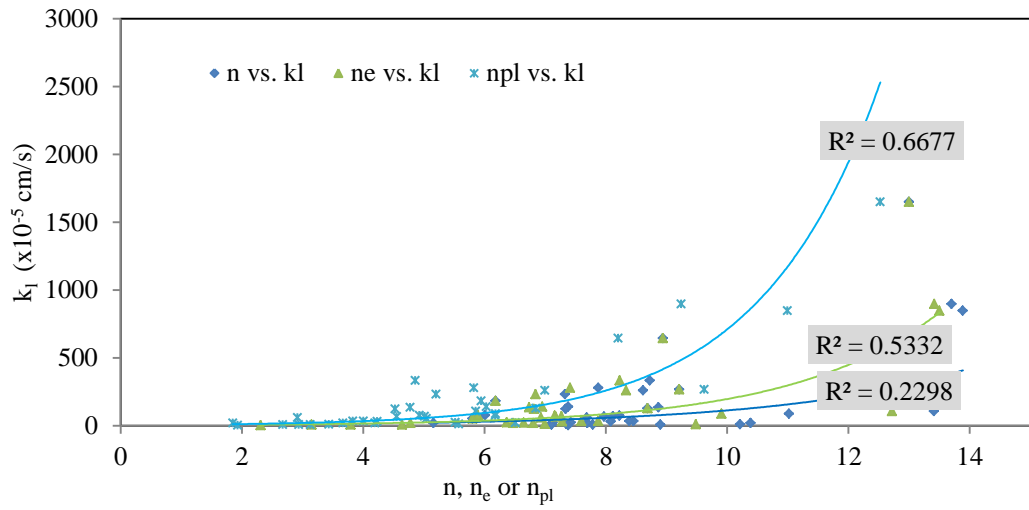


(a) Correlation of permeable pores with total pores and effective pores

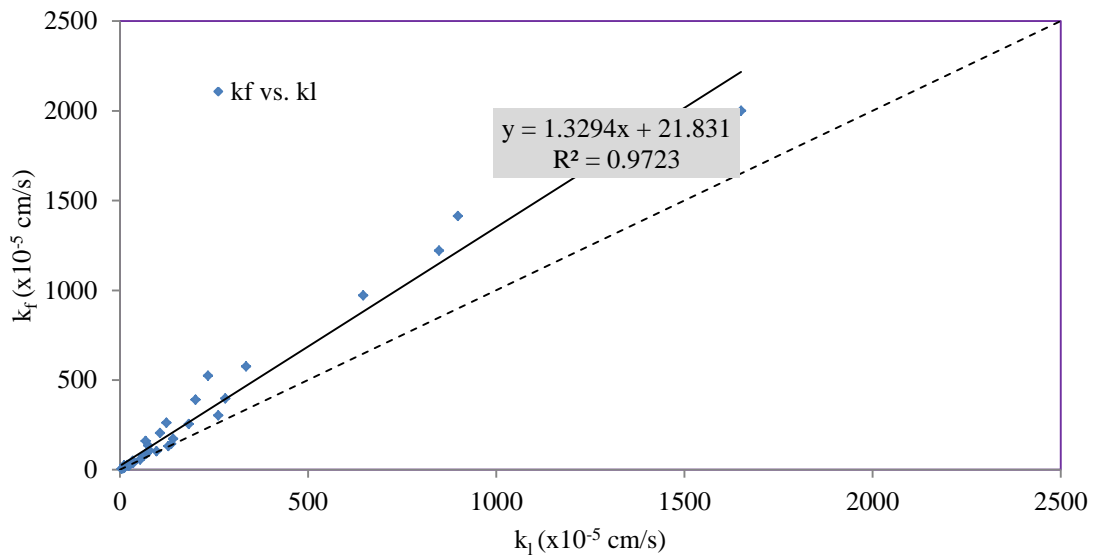


(b) Correlation between n_{pl1} and n_{pl2}

Figure 5.4 Different types of pores and their correlation.



(a) Relation of permeability with n , n_e , and n_{pl}



(b) Correlation between predicted and laboratory permeability

Figure 5.5 Different permeabilities and their relation with pores.

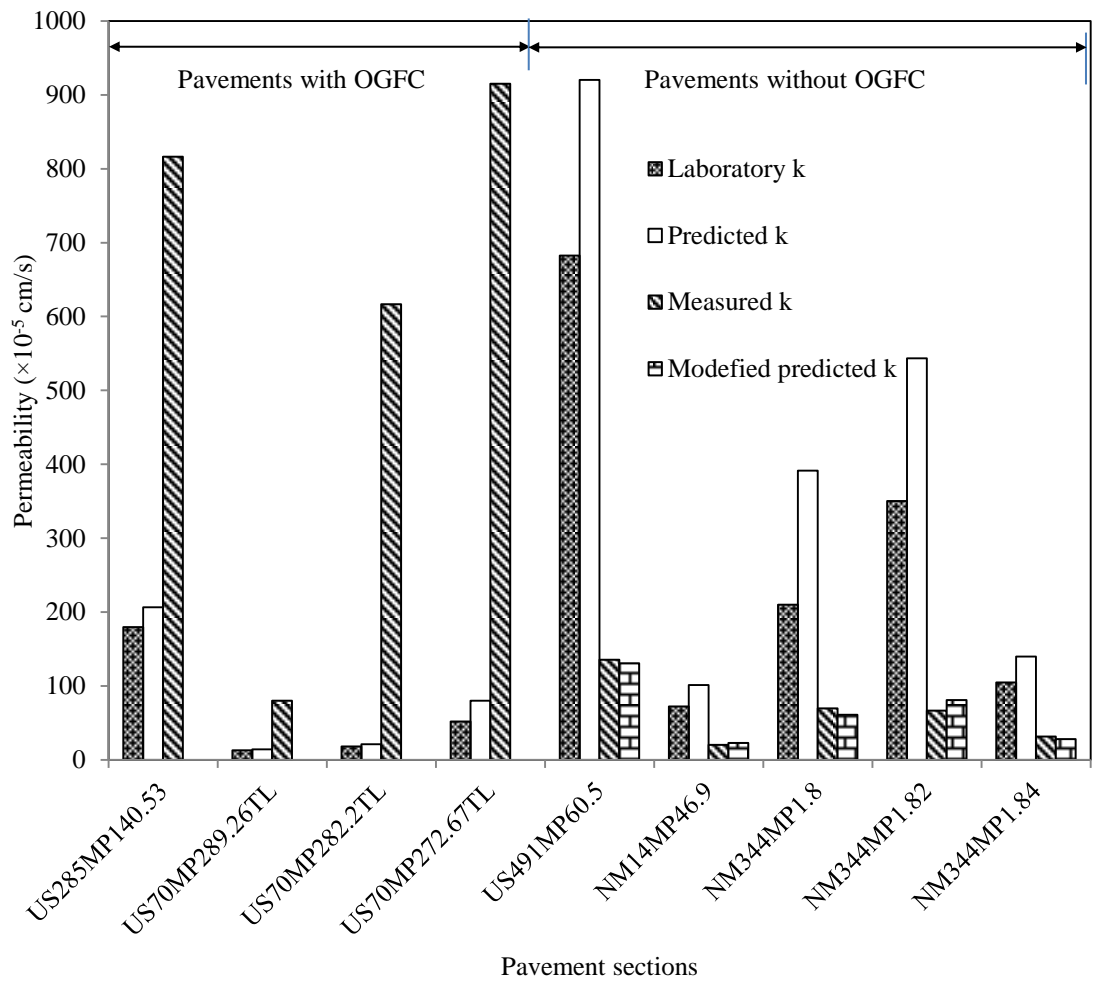
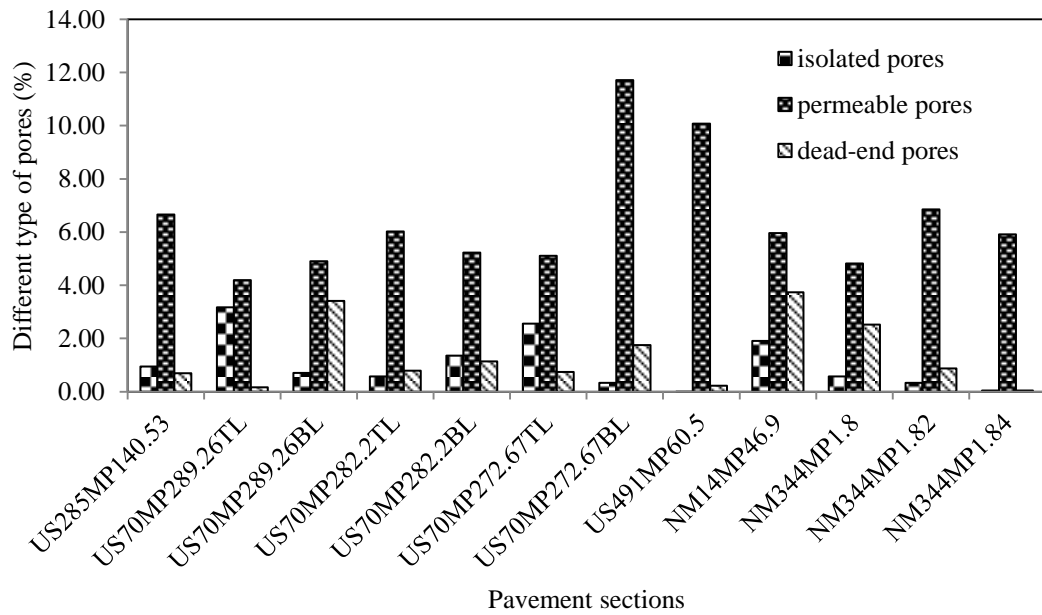
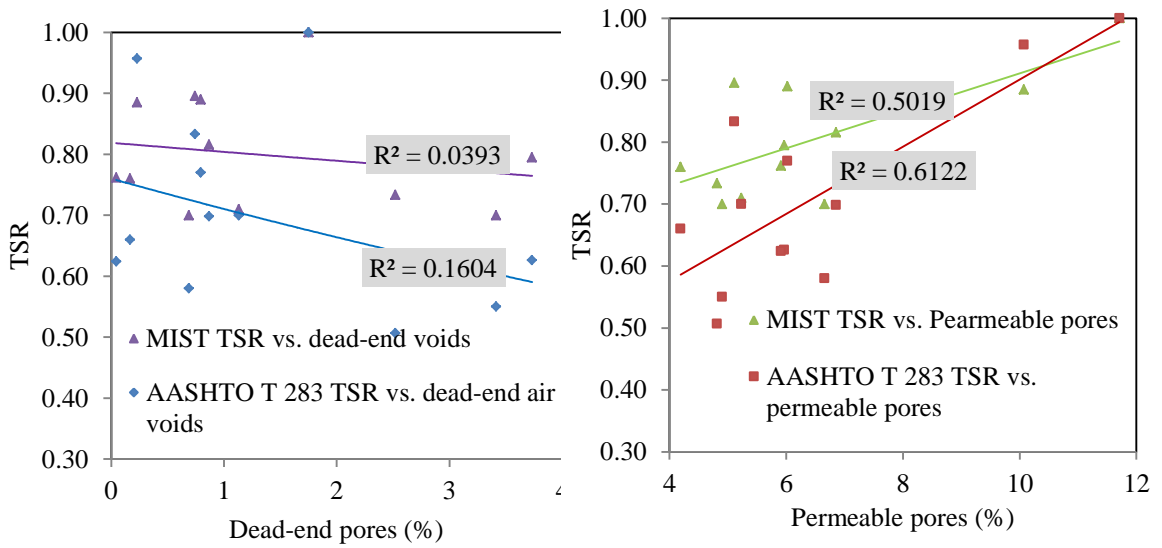


Figure 5.6 Comparison of field permeability with predicted and laboratory permeability.



(a) Different types of pores inside a pavement



(b) Correlation of TSR with dead end and permeable pores

Figure 5.7 Different types of pores and their relation with moisture damage.

CHAPTER 6

CONCLUSIONS AND RECOMMENDATIONS

6.1 SUMMARY

This study attempts to evaluate moisture damage and permeability characteristics of asphalt pavements.

Moisture damage is evaluated in the field and in the laboratory. In the field, moisture damage is initially identified by visual inspection of the pavements. Then visual inspection of the stripping of the cores identifies the moisture damage condition of the pavements more accurately and they are classified as good and bad performing pavements in terms of moisture damage condition. Cores are brought to the laboratory and TSR is determined by conventional the AASHTO T 283 and recently developed MIST procedures. Cores collected from good performing pavements yield reasonably higher TSR values than cores from the bad performing pavements, by both of the methods. Although some good performing pavements have less TSR and some bad performing pavements have more TSR value. Therefore none of the methods is very close to the reality. MIST TSR values are almost always higher than the AASHTO T 283 TSR. The frost action of pore water in case of the AASHTO T 283 is responsible for that.

As more permeability represents more mix surface accessible to water, it can be stated that permeability may influence moisture damage. To determine it, permeability of good and bad performing pavements are determined and compared. It is obtained that, bad performing pavements have higher permeability than good performing pavements. Therefore, pavements with higher permeability are more susceptible to water. To

quantify the correlation between permeability and moisture damage, TSR values obtained by the AASHTO T 283 and MIST are plotted against permeability. It is observed that permeability doesn't show any correlation with MIST TSR. The AASHTO T 283 TSR shows a better correlation. As damage in the AASHTO T 283 is mainly governed by the frost action of water, the more water a sample can hold, the more damage will occur. On the other hand, damage in MIST occurs due to cyclic loading at elevated temperature. For less permeable sample, it is still under cyclic loading elevated temperature and damage occurs.

Permeability is determined both in field and in the laboratory. In the field, permeability is determined on pavements with OGFC and without OGFC. In the laboratory, permeability of full depth samples and samples separated in layers are determined. All this permeability values are compared and it is tried to determine if there exists any correlation between field and laboratory permeabilities. It is obtained that field permeability cannot be correlated with laboratory permeability, as field permeability depends on lot of factors. For pavements with OGFC, field permeability values are much higher than laboratory permeability. Water may flow very quickly and laterally through OGFC yielding higher permeability in the field. For pavements without OGFC, field permeability values are much less than laboratory permeability of top layer. The discontinuity of flow path and tack coat and seal coat may reduce the flow to a great extent.

As field permeability may yield inaccurate results, it is necessary to determine it alternatively. An analytical approach to determine field permeability by testing core in the laboratory is introduced in this study. The first step of this method is to determine

permeable porosity using conventional tracer method. It is determined because permeability depends only on permeable pores. Dead end and isolated pores have no contribution to flow. Permeable pores are more in the field than in the laboratory because in the laboratory specimen is confined at sides and there is no flow in the lateral direction. Therefore, lateral permeable pores must be added to laboratory permeable pores to determine field permeable pores. The analytical method introduced in this study describes a procedure to determine field permeable pores. When field permeable pores are known, field permeability can be determined using two models developed in this study. Both models show very close results. The proposed models yield field permeability more than laboratory permeability, which was expected. In case of pavements with OGFC, the predicted permeability from model is less than the permeability determined in the field. This is expected as field permeability tests on OGFC overestimate the flow. In case of pavement without OGFC, the predicted permeability from the models is more than the permeability determined in the field. It is also expected as field permeameter underestimates the flow in this case. Therefore it can be concluded that, the developed models yields reasonably well results. To accommodate field boundary conditions like OGFC and different coats, a shift factor is proposed for predicted permeability. Shift factor works very well for pavements without OGFC.

Almost all the previous studies focused on the permeability and total pores (air voids) correlation, as it can be determined easily. As isolated or dead end pores have no contribution to flow, the correlation is not realistic or feasible. This study correlates permeability with permeable pores, which gives much better correlation than correlation with total pores.

Total pores consist of the distinct type of pores: permeable pores, dead end pores and isolated pores. This study determines these three types of pores. Permeable pores drain out water quickly whereas dead end pores holds the water. Therefore these two quantities may have correlation with moisture damage. This study shows that moisture damage decrease with the increase of permeable pores and increase with the dead end pores. This is expected because; permeable pores drain out water causing less interaction between water and pavement. Dead end pores holds the water causing more damage due to pumping action.

6.2 CONCLUSIONS

The following conclusions can be made from this study:

- Both field and laboratory permeability of good performing sections are less than the permeability of bad performing sections.
- Cores from good performing sections have higher TSR values than cores from bad performing section as determined by the AASHTO T 283 and MIST procedures. The MIST TSR in most of the cases higher than the AASHTO T 283 TSR indicating less damage in MIST. For samples with very low air voids or permeability, more damage occurs in the MIST than the AASHTO T 283. Although MIST TSR doesn't show any good correlation with permeability, the AASHTO T 283 TSR shows a better correlation.
- Permeability is better correlated with permeable porosity than total porosity and effective porosity, as it eliminates dead end and isolated pores which have no contribution to flow.

- Moisture damage decreases with the increase of permeable pores and increases with the increase of dead end pores.
- A new analytical approach to determine field permeable pores as well as field permeability by testing cores in the laboratory is developed in this study. The model permeability is always greater than laboratory permeability as it includes lateral flow. Pavement with and without OGFC overestimates and underestimates permeability respectively. A shift factor of 0.132 with an intercept is applied to match model permeability with field permeability for pavements without OGFC.

6.3 RECOMMENDATIONS

The following studies can be made further to establish this study:

- Hamburg wheel tracker may be used to determine the moisture susceptibility of the mix. As it applies cyclic loading and wheel pressure similar to the field, this prediction may be more useful and comparable with other test methods.
- A small single layer test pavement can be constructed over a highly permeable sand layer with the facility of saturation. Field permeability test on that pavements may give very accurate prediction, as there is no OGFC, tack coat, seal coat and discontinuity of flow path. Laboratory permeability of the cores collected from this pavement can be used to verify the model proposed in this study.

REFERENCES

- AASHTO Standard T 283. Standard Method of Test for Resistance of Compacted Hot Mix Asphalt (HMA) to Moisture-Induced Damage. AASHTO Guide, Washington, DC, 2007.
- Ahmad, M., and R. A. Tarefder. *Addressing Permeability of SuperPave Mixes In New Mexico*. 3rd Quarter FY13, ORA 456-340, Research Bureau, New Mexico Department of Transportation, 2013, pp. 1-43.
- Al-Omari, A., L. Tashman, E. Masad, A. Cooley, T. Harman. 2002. "Proposed Methodology for Predicting HMA Permeability." *J. Assoc. Asphalt Pav. Technology*, 71.
- ASTM D 6752. Standard Test Method for Bulk Specific Gravity and Density of Compacted Bituminous Mixtures Using Automatic Vacuum Sealing Method. American Society for Testing and Materials, PA.
- ASTM D 6857: Standard Test Method for Maximum Specific Gravity and Density of Bituminous Paving Mixtures Using Automatic Vacuum Sealing Method.
- Bear, J. *Dynamics of Fluids in Porous Media*. American Elsevier Publishing Company. Inc., 1972.
- Bhattacharjee, S., and R. B. Mallick. An Alternative Approach for the Determination of Bulk Specific Gravity and Permeability of Hot Mix Asphalt (HMA). *International Journal of Pavement Engineering*. Vol 3, No. 3, 2002, pp. 143-152.
- Brown, E. R., M. R. Hainin, A. Cooley, and G. Hurley. *Relationship of Air Voids, Lift Thickness, and Permeability in Hot Mix Asphalt Pavements*. NCHRP Report 531, 2004.

- California Test 341: Method of Test for Measuring the Permeability of Bituminous Pavements and Seal Coats.
- Celik, O.N., (2005) “Air Permeability of Asphalt Concrete Made with Shredded-Tire Rubber- Modified Binders and its Relationship with Porosity.”J. of Testing and Evaluation, 33(4), 217–221.
- Choubane, B., Page, G.C., and Musselman, J.A. (2007).“Effects of Water Saturation Level on Resistance of Compacted Hot-Mix Asphalt Samples to Moisture-Induced Damage.”In Trans. Res. Rec. J. of the Trans. Res. Board, 1723(2000), TRB, National Research Council, Washington, D.C., 97–106.
- Cooley, Jr., L. A., B. D. Prowell, and E. R. Brown. *Issues Pertaining to the Permeability Characteristics of Coarse Graded SuperPave Mixes*. 2002 Annual Meeting of the Association of Asphalt Paving Technologists.
- Cooley Jr., L.A. 1999. “Permeability Of Superpave Mixtures: Evaluation of Field Permeameters” NCAT Report No. 99-1.
- FM 5-565: Florida Method of Test for Measurement of Water Permeability of Compacted Asphalt Paving Mixtures.
- Gogula, A. K., M. Hossain, and S. A. Romanoschi. *A Study of Factors Affecting the Permeability of Superpave Mixes in Kansas*. Final report, Report No. K-TRAN: KSU-00-2, 2004.
- Hainin, M. R., L. A. Cooley, Jr., and B. D. Prowell. *An Investigation of Factors Influencing Permeability of Superpave Mixes*. TRB 2003 Annual Meeting.

- Hall, K. D., and H. G. Ng. Development of Void Pathway Test for Investigating Void Interconnectivity in Compacted Hot-Mix Asphalt concrete. *Journal of Transportation Research Board*, Volume 1767, 2001, pp. 40-47.
- Harris, C.H. 2007. "Hot Mix Asphalt Permeability: Tester Size Effect and Anisotropy." MS thesis, Virginia Polytechnic Institute and State University.
- Hicks, R. G. (1991). *Moisture Damage in Asphalt Concrete: Synthesis of Highway Practice*, NCHRP Report 175.
- InstroTek, Inc. *Moisture Induced Sensitivity Test*. Raleigh, NC, 2012.
- Jones, S.C. 1997. "A Technique for Faster Pulse Decay Permeability Measurements in Tight Rocks" *SPE formation evaluation*, SPE 28450.
- Jury, W.A., and R. Horton. *Soil Physics*. 6th Edition, John Wiley and Sons, Inc., 2004.
- Kanitpong, K., H. Bahia, J. Russell, and R. Schmitt. Predicting Field Permeability from Testing Hot-Mix Asphalt Specimens Produced by Superpave Gyratory Compactor. *Journal of Transportation Research Board*, No.1929, 2005, pp. 52-58.
- Kim, S., and Coree, B.J. (2005).Evaluation of Hot Mix Asphalt Moisture Sensitivity Using the Nottingham Asphalt Test Equipment. IHRB Project TR-483.
- Koponen, A., M. Kataja, and J. Timonen. Permeability and Effective Porosity of Porous Media. *The American Physical Society*, Vol. 56, No. 3, 1997, pp. 3319-3325.
- Liang, R.Y. (2008).Refine AASHTO T283 Resistance of Compacted Bituminous Mixture to Moisture Induced Damage for Superpave.Final Report FHWA/OH-2008-1.

- Liang, Z., M. A. Ioannidis, and I. Chatzis. Permeability and Electrical Conductivity of Porous Media from 3D Stochastic Replicas of the Microstructure. *Chemical Engineering Science*, Vol. 55, Issue 2000, 2000, pp. 5247-5262.
- Masad, E., Castelblanco, A., and Birgisson, B. (2006). "Effects of air void size distribution, pore pressure, and bond energy on moisture damage." *J. of Testing and Evaluation*, 34(1), 15–23.
- Masad, E., B. Birgisson, A. Al-Omari, and A. Cooley, 2002. "Analysis Of Permeability And Fluid Flow In Asphalt Mixes" *A Paper Submitted to the 82nd Annual Transportation Research Board for Presentation and Publication.*
- Mallick, R. B., L. A. Cooley, Jr., M. R. Teto, R. L. Bradbury, and D. Peabody. *An Evaluation of Factors Affecting Permeability of Superpave Designed Pavements.* NCAT Report 03-02, 2003.
- Menard, J., and J. A. Croveti. Comparative Analysis of Field Permeability Testing of Compacted Hot-Mix Asphalt Pavements. *Journal of Transportation Research Board*, No.1946, 2006, pp. 147–156.
- Mercado, E.A. (2007). "Influence of fundamental material properties and air void structure on moisture damage of asphalt mixes," PhD Thesis submitted to Texas A&M University.
- Mogawer, W.S., Mallick, Teto, M.R., and Crockford, W.C. (2002). Evaluation of Permeability of Superpave Mixes. NETCR 34, New England Transportation Consortium, North Dartmouth, MA, Project No. NETC 00-2.
- Mohammad, L. N., A. Herath, and B. Huang. *Evaluation of Superpave Paving Mixture.* TRB 2003 Annual Meeting.

- Ranieri, V., M. C. Antonnaci, G. Ying, and J. J. Sansalone. Application of Kozeny-Kovacs Model to Predict the Hydraulic Conductivity of Permeable Pavements. *Journal of Transportation Research Board*, No. 2195, 2010, pp. 168-176.
- Retzer, N. 2008. "Permeability Research With the ROMUS Air Permeameter" *Colorado Department of Transportation*, Final Report, Report No. CDOT-2008-5.
- OHD L-44: Method Of Test For Measurement Of Water Permeability Of Compacted Paving Mixtures.
- Omari, A. A. Analysis of HMA Permeability through Microstructure Characterization and Simulation of Fluid Flow in X-Ray CT Images. Dissertation submitted to Texas A&M University, 2004.
- Retzer, N. *Permeability Research with the Romus Air Permeameter*. Report to Colorado DOT, Report No. CDOT-2008-5, 2008.
- Rogowski, A. S. Flux Density and Breakthrough Times for Water and Tracer in A Spatially Variable, Compacted Clay Soil. *Journal of Contaminant Hydrology*, Vol.3, 1988, pp. 327-348.
- Stephens, D. B., K. Hsu, M. A. Prieksat, M. D. Ankeny, N. Blandford, T. L. Roth, J. A. Kelsey, and J. R. Whitworth. A Comparison of Estimated and Calculated Effective Porosity. *Hydrology Journal*, Vol.6, 1998, pp. 156-165.
- Tarefder, R. A., L. White, and M. Zaman. Neural Network Model for Asphalt Concrete Permeability. *Journal of Materials in Civil Engineering*, Vol. 17, No. 1, 2005, pp. 19-27.
- TEX 246-F: Test Procedure for Permeability or Water Flow of Hot Mix Asphalt.

- Torres, A.C. (2004). Probabilistic Analysis of Air Void Structure and Its Relationship to Permeability and Moisture Damage of Hot Mix Asphalt. MS Thesis submitted to Texas A&M University.
- Vivar, E., and J. E. Haddock. Hot Mix Asphalt Permeability and Porosity. *Journal of the Association of Asphalt Paving Technologists*. Vol. 76, 2007, pp. 952-979.
- Williams, S.G. 2006. "A Comprehensive Study of Field Permeability Using the Vacuum Permeameter." MBTC-2054.
- Willoughby, K. A., J. P. Mahoney, L. M. Pierce, J. S. Uhlmeier, K. W. Anderson, S. A. Read, S. T. Muench, T. R. Thompson and R. Moore 2001 "Construction-Related Asphalt Concrete Pavement Temperature Differentials and the Corresponding Density Differentials" Research report for Washington DOT.
- Yeh, Y., C. Lee, and S. Chen. A Tracer Method to Determine Hydraulic Conductivity and Effective Porosity of Saturated Clay under Low Gradient. *Ground Water*, Vol.38, 2000, pp. 522-529.